

HRTF measurement for accurate identification of binaural sound localization cues

Authors: Gyeong-Tae Lee, Sang-Min Choi, Byeong-Yun Ko, Yong-Hwa Park*

Center for Noise and Vibration Control, Department of Mechanical Engineering
Korea Advanced Institute of Science and Technology (KAIST)
Daejeon 34141, Korea

E-mail: hansaram@kaist.ac.kr (G. T. Lee), cyanray1500@kaist.ac.kr (S. M. Choi), b.y.ko@kaist.ac.kr (B. Y. Ko), yhpark@kaist.ac.kr (Y. H. Park)

Running title: HRTF measurement for accurate sound localization cues

Number of manuscript pages: 40

Number of figures: 27

Number of tables: 1

*All correspondences concerning this paper should be addressed to:

Yong-Hwa Park, Prof.

Dept. of Mechanical Eng., KAIST

Daejeon 34141, Korea

(Phone) +82-42-350-3235

(Mobile) +82-10-3326-7337

(E-mail) yhpark@kaist.ac.kr

Abstract

Although various research institutes have measured head-related transfer functions (HRTFs), the standards for system design, measurement, and post-processing have often been unclear or inaccurate. This paper presents accurate and practical methods for the major issues of HRTF database construction, especially on loudspeaker design, measurement of the origin transfer function at the head center, selection of time window interval, and compensation for non-causality of ipsilateral HRTF. Then, the effect of each method on binaural sound localization cues was investigated. To achieve maximum bandwidth in the limited space, a 1-way sealed speaker module was designed by simulating its frequency response based on electro-acoustics. The origin transfer function was measured with 0° on-axis microphone to ensure its non-directionality. To measure the origin transfer function with the minimized number of microphone redirections, the entire elevation range of the speaker array was divided into sub-sections considering the omni-directional range of the microphone. Then each speaker module was measured with the microphone pointing to the center of the corresponding sub-section. When measured with a 90° off-axis microphone, the magnitude response of the origin transfer function fluctuates and decreases with increasing frequency, which causes erroneous spectral cues of HRTF. To reduce the size of the HRTF database and exclude reflections due to measurement equipment, the start and end points of the time window were set considering the propagation delay and the reflection of each impulse response. Each binaural and origin impulse response is clipped by the time window, and HRTF is computed by complex division between the binaural and origin transfer functions. To prevent the discontinuity due to the non-causality of ipsilateral HRTFs, all head-related impulse responses (HRIRs) are circular shifted by a time delay longer than the head radius divided by the speed of sound. The discontinuity of ipsilateral HRTFs causes an excessive time difference between left and right HRIRs. Finally, interaural time difference (ITD), interaural level difference (ILD), spectral cue (SC), and horizontal plane directivity (HPD) were extracted from the HRTFs to examine the effect of each method on binaural sound localization cues. MATLAB codes and resulting HRTF database are available at GitHub (<https://github.com/hansaram80/HRTF-construction>).

Keywords: Head-related transfer function (HRTF); Interaural time difference (ITD); Interaural level difference (ILD); Spectral cue (SC); Horizontal plane directivity (HPD)

1. Introduction

Humans analyze the auditory scene by localizing and recognizing surrounding sound sources. The human brain can localize sounds by taking advantage of the way sounds are modified on their way to the ears, specifically how they are modified differently between the two ears. When a sound wave in a certain direction reaches both ears, it interacts with the torso, head, and pinna, causing temporal and spectral transformations. The resulting effects provide meaningful clues about the location of the sound source. In duplex theory [1], Lord Rayleigh suggests that the human ability to localize sounds depends on interaural time difference (ITD) and interaural level difference (ILD), which actually influence azimuth localization. In addition, the pinna generates direction-dependent spectral cue (SC) that can be used by the brain to estimate source elevation. Although there is no simple relationship between direction and sound localization cues, the human brain can use these cues to accurately estimate the location of sound sources. Therefore, to simulate an acoustic scene with sound sources in different directions, the sound sources must be modified according to their directions. In binaural audio, this simulation is implemented by the direction-dependent acoustic filters, referred to as head-related impulse responses (HRIRs) in time domain, or head-related transfer functions (HRTFs) in frequency domain, respectively. An HRTF is a frequency response describing the sound transmission from a free field source position to a point in the ear canal [2–6]. HRTFs can be measured in the form of linear time-invariant filters and synthesized by various models for real-time applications [7].

Since HRTFs contain all binaural and spectral cues for sound source localization (including ITD, ILD, SC, etc.), they play an essential role in binaural rendering for virtual auditory display (VAD) and 3D audio reproduction over headphones or loudspeakers, especially in immersive listening experience for virtual reality (VR) and augmented reality (AR) scenarios [8,9]. Recently, HRTFs have been used as a development dataset for deep learning-based binaural sound source localization (BSSL), which aims to localize sound sources using two microphones by mimicking the principle of binaural hearing [10,11]. Contrary to VAD, which implements binaural rendering by convolving an input signal with left and right HRIRs of a certain direction, deep learning-based BSSL extracts sound localization cues (HRTF information) from input signals of a two-sensor array to estimate the direction of sound sources. Therefore, HRTF learning-based BSSL is suitable for the sound source localization method of humanoid robots with two ears.

In recent decades, various laboratories have constructed HRTF databases to support their own research. Some databases are publicly available for scientific or commercial purposes [12–19]. Although methods for measuring HRTFs have existed for decades, there is no common methodology used by laboratories around the world, and the criteria for measurement and post-processing are still often unclear or inaccurate. In particular, loudspeaker design, measurement of the origin transfer

function at the head center, selection of time window interval, and compensation for non-causality of ipsilateral HRTF, which are commonly encountered in the HRTF measurement process, are unclear or inaccurate.

A considerable number of previous studies have measured HRTFs using commercial loudspeakers [12,14–16,20–28]. Since commercial loudspeakers are designed for high sound quality, a vent or passive radiator is installed to expand its low-frequency band, or a tweeter is added to a mid-range speaker to enhance its high-frequency response. Therefore, they emit sound from multiple sources rather than a single source. Since accurate measurement is possible when there is a single sound source in each direction, commercial speakers are not suitable for HRTF measurement. Although other studies made sealed speaker modules using a single speaker driver, they did not sufficiently reproduce the frequency band of interest [29–32]. This is because each speaker module was not designed in consideration of its speaker driver's electro-acoustic characteristics in a given volume. For a circular baffle with a speaker driver in the center [33], there will be many dips and peaks in the frequency response whenever the edge is apart from the center by multiples of a half-wavelength. Since the source-to-edge distances are all equal, the on-axis response for a circular baffle exhibits worst-case edge diffraction [34]. In case of an unbaffled speaker driver [35], the sound from the front and rear side of the speaker diaphragm causes destructive interference, reducing the low to mid-range frequency level.

According to Blauert [36], a free-field HRTF is calculated by dividing a binaural transfer function (BTF) by an origin transfer function (OTF) of the head center with the head absent to exclude the influence of the measurement system. For reference, time domain response of the BTF is binaural impulse response (BIR), and that of the OTF is origin impulse response (OIR). In previous works [12,22–24,37,38], only BTFs were measured and incorrectly called HRTFs. BTFs will be significantly different from the actual HRTFs unless the bandwidth of frequency response of the measurement system, especially the speaker module, is sufficiently wide and its tonal balance is ensured. In previous works [12,26,29,40], an OTF was measured with a microphone different from that used for BTF measurement. In this case, even if each BTF is normalized to the OTF, the response difference between the microphones affects the accuracy of HRTFs. In addition, since microphones used for HRTF measurement have directivity, an OTF should be measured by pointing a microphone toward the acoustic on-axis of each speaker module to obtain a correct response of the total measurement system. In previous studies related to the OTF measurement, some studies pointed the microphone toward the acoustic on-axis of a sound source [31,32,40,41], while others tilted the microphone 90° off-axis from a sound source [21,29,39]. When a microphone is tilted at right angles to the speaker on-axis, there is no directivity in the circumferential direction of the microphone diaphragm, but there is directivity in its radial direction, which breaks down its high frequency response [42]. Therefore, normalizing BTFs

with the OTF of 90° off-axis results in inaccurate HRTFs with overly emphasized high frequencies.

In BIR and OIR, the time interval containing essential information is only a few milliseconds. Therefore, a window function is needed to extract the essential sections from BIR and OIR. In the OIR, its maximum sample position is fixed because the distance between the microphone and the speaker module is constant, whereas in the BIR, its maximum sample position changes because the distance from the microphone varies according to the direction of the speaker module. Several studies applied a window function considering the propagation delay of a sound source [8,12,16,29], whereas other studies applied a window function to remove the reflection from the measurement system [14,22,31,32,37,39,40,43]. However, they did not clearly provide the setting criteria for both the start and end points of the most essential time interval. The start point setting is important to preserve the initial main peaks of BIR and OIR and their pre-peak ripples, and the end point setting is important to prevent comb filtering effects due to reflection. Iida [6] set the start point of a window function based on the maximum absolute value of the front BIR. However, in the case of ipsilateral BIRs, where onset starts earlier than the front BIR, the initial main peaks could be lost. In Ref. [18,19,26], a Hanning window was used instead of a rectangular window to mitigate the effect of reflection, but the location of the start and end points was not clearly presented. Thus, the main part of the impulse response could be distorted by the transient region of the Hanning window. Some studies applied a window function so that the center of the window function is located at the maximum sample position of BIRs [38,41]. Since impulse responses contain key information after the maximum amplitude, locating the center of window function at the maximum amplitude leaves too much unnecessary information before it.

A pair of left and right HRTFs is computed by complex division of the corresponding pair of BTFs by OTFs. Here, it is important to note that ipsilateral HRTFs are non-causal by the mathematical definition of HRTF because the ipsilateral ear is closer to the sound source than the head center. On the other hand, contralateral HRTFs are causal because the contralateral ear is farther from the sound source than the head center. In general, derived HRTFs are converted into HRIRs in time domain through inverse Fourier transform (IFT) when HRTFs are stored in a database. Since an ipsilateral HRIR is non-causal, the maximum sample of the ipsilateral HRIR should precede 0 seconds. However, the maximum sample appears later in the ipsilateral HRIR. This is because the Fourier transform treats time series data as a repeating periodic signal. Therefore, additional post-processing is required due to the discontinuity of ipsilateral HRIRs. Møller [3] noted that some HRTFs are non-causal, but did not suggest a post-processing procedure to secure causality. Xie [5] suggested a method to ensure causality only when the denominator of a HRTF is a non-minimum phase function. However, he did not present how to compensate for the non-causality of ipsilateral HRTFs. Iida [6] systematically summarized the procedure for obtaining HRTFs, but did not mention the non-causality issue of ipsilateral HRIRs and

how to compensate for it. In other HRTF measurements [12–19, 21–25, 30, 31, 38–40], non-causality issues and methods to guarantee causality were also not presented.

In this paper, accurate and practical methods are presented for the major issues of HRTF database construction such as wideband speaker module design, OTF measurement, selection of time window interval, and compensation for non-causality of ipsilateral HRTFs. Then, by analyzing ITD, ILD, SCs, and horizontal plane directivity (HPD) in the derived HRTF, it is examined whether binaural sound localization cues are accurately identified by the presented methods. The rest of the paper is organized as follows. Section 2 defines HRTFs after presenting the adopted coordinate system and head transverse planes. Section 3 explains a speaker array structure, the configuration of the HRTF measurement system, and a practical electro-acoustic based speaker module design procedure. In section 4, a process used to measure raw transfer functions, especially on OTFs, is described in detail, and a guide for setting the start and end points of a time window is presented. Section 5 deals with compensation for non-causality of ipsilateral HRTFs. Then the time and frequency domain characteristics of the derived HRTFs are presented and discussed. Section 6 analyzes the sound localization cues of HRTFs by using ITD, ILD, SCs, and HPD. Finally, the effects of the presented methods on the accurate identification of binaural sound localization cues are discussed and concluded in section 7. BTF and OTF measurement results, MATLAB codes for building HRTF database, and data files about derived HRTFs and binaural sound localization cues are available on GitHub (<https://github.com/hansaram80/HRTF-construction>).

2. Definition of HRTFs

2.1. Spherical coordinate system and head transverse planes

The spherical coordinate system and head transverse planes for specifying the location of a sound source are shown in Fig. 1.

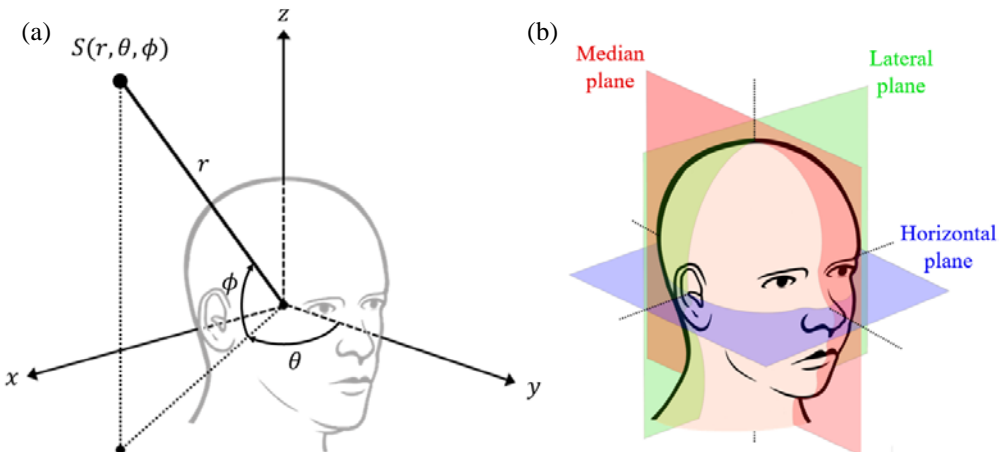


Fig. 1. Illustrations of (a) a spherical coordinate system and (b) head transverse planes.

In Fig. 1(a), the origin of the coordinate system is an imaginary point at the center of the head between the entrances to the two ear canals. The x , y , and z -axes point from the origin to the right ear, front, and top of the head, respectively. In Fig. 1(b), the three specific planes of space are defined by these three axes. The horizontal plane is the xy -plane that contains the x and y -axes. The median plane is the yz -plane that contains the y and z -axes. The lateral plane is the xz -plane that contains the x and z -axes. The three planes are perpendicular to each other and intersect at the origin. The direction vector pointing from the origin to the sound source indicates the position (r, θ, ϕ) of the sound source in space. The azimuth θ is the angle between the y -axis and the horizontal projection of the direction vector, clockwise being positive and counterclockwise being negative ($-180^\circ < \theta \leq +180^\circ$), where $-90^\circ, 0^\circ, +90^\circ$, and $+180^\circ$ indicate the left, front, right, and back directions respectively in the horizontal plane. The elevation ϕ is the angle between the horizontal plane and the direction vector of the sound source, with a positive upward direction and a negative downward direction ($-90^\circ \leq \phi \leq +90^\circ$), where $-90^\circ, 0^\circ$, and $+90^\circ$ represent the bottom, front and top directions respectively in the median plane.

2.2. Derivation of HRTFs based on measured transfer functions

The sound emitted from a sound source is diffracted and reflected from the torso, head, and pinna, and then reaches both ears. In Fig. 2, the sound transmission process from the sound source to the both ears can be regarded as a linear time-invariant (LTI) process. HRTFs are the acoustic transfer functions of the LTI process and account for the overall acoustic filtering effect by human anatomy. A pair of HRTFs of the left and right ears for an arbitrary sound source is defined as

$$H_{L,R}(r, \theta, \phi, f, s) = \frac{P_{L,R}(r, \theta, \phi, f, s)}{P_0(r, f)}, \quad (1)$$

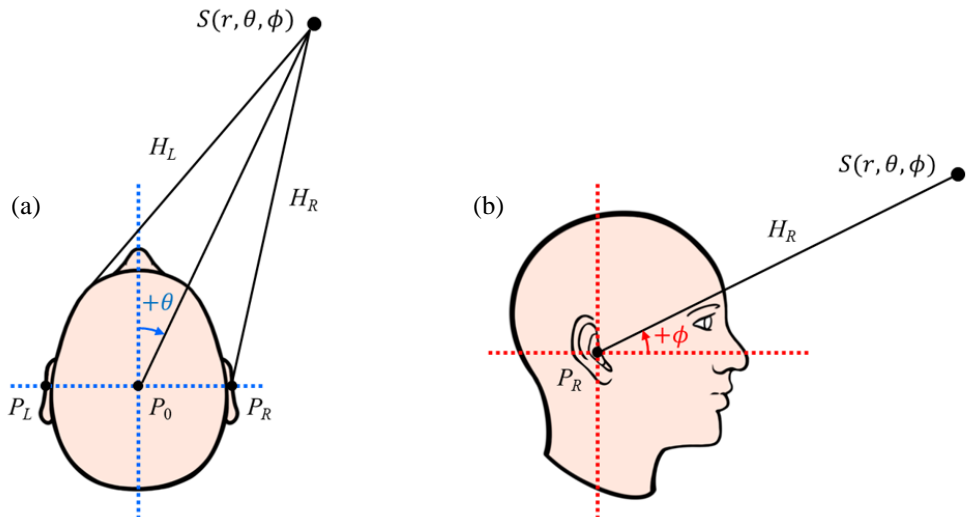


Fig. 2. Diagrams of sound transmission from a sound source to the both ears: (a) top view; (b) side view.

where $P_{L,R}$ is the complex-valued sound pressure in frequency domain at the entrance of the ear canal of subject, and P_0 is the complex-valued sound pressure in frequency domain at the center of the subject's head when the subject does not exit. The subscripts L and R denote the left and right ears, f refers to frequency, and s refers to a set of parameters related to the dimensions of the subject's anatomical structures.

Although Eq. (1) is expressed in terms of sound pressure, when actually calculating HRTFs, the measured transfer function between a loudspeaker and a microphone is used, not the sound pressure. Therefore, it is useful to express HRTFs based on the measured transfer functions. Eq. (1) can be expanded as follows:

$$H_{L,R}(r, \theta, \phi, f, s) = \frac{P_{L,R}(r, \theta, \phi, f, s) \cdot Y(\phi, f)/X(f)}{P_0(r, f) \cdot Y(\phi, f)/X(f)} = \frac{\tilde{P}_{L,R}(r, \theta, \phi, f, s)/X(f)}{\tilde{P}_0(r, \phi, f)/X(f)}, \quad (2)$$

where $Y(\phi, f)$ is the frequency response including digital-to-analog converter (DAC), speaker amplifier, speaker module at elevation ϕ in a vertical speaker array, microphone, microphone conditioner, and analog-to-digital converter (ADC), and $X(f)$ is the frequency response of an input signal. As result, in the last term in Eq. (2), the measured sound pressure at the entrance of the left or right ears can be denoted by $\tilde{P}_{L,R}(r, \theta, \phi, f, s)$, and the measured sound pressure at the head center (the origin of the coordinate system) can be denoted by $\tilde{P}_0(r, f)$. The numerator of Eq. (2) is the BTF as the sound transfer function between the sound source and the entrance of the left or right ear canal, and the denominator is the OTF as the sound transfer function between the sound source and the origin of the coordinate system. The BTF and OTF are respectively defined as follows:

$$G_{L,R}(r, \theta, \phi, f, s) = \tilde{P}_{L,R}(r, \theta, \phi, f, s)/X(f), \quad (3)$$

$$G_0(r, \phi, f) = \tilde{P}_0(r, \phi, f)/X(f). \quad (4)$$

In general, when measuring HRTFs, both s and r are constant because the measurement subject is predetermined and the distance of a speaker module from the origin is also fixed for a specific measurement setup. Therefore, based on the BTF and OTF to be measured, the HRTF is defined as

$$H_{L,R}(\theta, \phi, f) = \frac{G_{L,R}(\theta, \phi, f)}{G_0(\phi, f)}. \quad (5)$$

3. Design of HRTF measurement system

3.1. Configuration of HRTF measurement system

The HRTF measurement system used in this study was designed to measure HRTFs not only on artificial heads but also on humans. However, since this paper was written to present accurate methods for several common issues encountered in the process of building a HRTF database, the measurement subject was limited to a dummy head, Brüel & Kjær (B&K) HATS Type 4100. The HRTF measurement

system is designed to be installed in the anechoic chamber at Korea Advanced Institute of Science and Technology (KAIST). The size of the KAIST anechoic chamber is 3.6 m in width, 3.6 m in length, and 2.4 m in height, and the cut-off frequency is 100 Hz. Thus, the frequency band of interest of the HRTF measurement system was bounded from 120 Hz to around 20 kHz. In addition, the distance r from the center of the head of the dummy head to the speaker module was set to 1.1 m in consideration of the height of the anechoic chamber. When the distance r exceeds 1 m, the frequency characteristics of HRTFs are not affected [6]. For reference, when the distance r is greater than 1 m, the HRTFs become distance-independent and are called far-field HRTFs. On the other hand, when the distance r is less than 1 m, the HRTFs become distance-dependent and are called near-field HRTFs.

The range of the sound source azimuth θ was set from -180° to $+180^\circ$. The range of the sound source elevation ϕ was set from -40° to $+90^\circ$ in consideration of the height of the anechoic chamber. According to several studies [44,45], the angular resolution of a HRTF database should be less than 5° in the horizontal plane and less than 10° in the vertical plane. Therefore, the azimuth and elevation resolutions of the HRTF measurement system were set to 5° , respectively. A turntable driven by a servomotor was designed to realize the azimuth resolution of 5° precisely. As shown in Fig. 3, the measurement subject is mounted on the turntable and rotates so that the speaker array faces the azimuth angle set by the direction-of-arrival (DOA) controller. Since the rotating shafts of the servomotor and turntable are connected by a timing belt, accurate azimuth control of a sound source is possible. To realize the 5° elevation resolution, as shown in Fig. 3, the semicircular speaker array composed of speaker modules spaced 5° apart to each other being distributed from -40° to $+90^\circ$ was designed. If an elevation angle is set in the DOA controller, only the switch connected to the corresponding speaker module is turned on in the speaker selector, enabling accurate elevation control of the sound source. Finally, the total number of sound source locations where HRTFs are measured is 1,944 (72 points in azimuth \times 27 points in elevation).

As shown in Fig. 3, raw transfer functions, BTFs and OTFs, are measured through the audio interface (Audiomatica CLIO FW-02) connected to the host computer via USB 2.0. For reference, the sampling rate of the audio interface is 48 kHz, and the sample size of a measured impulse response is 4,096. In addition, the output signal of the audio interface for full frequency excitation was set as a maximum length sequence (MLS). The MLS from the audio interface is amplified through the speaker amplifier (YBA Heritage A200) and then reproduced as a sound source through the speaker module selected by the speaker selector. The acoustic signal input to the microphone of the dummy head is amplified through the microphone conditioner (B&K NEXUS) and then input to the audio interface. The transfer function is calculated through ensemble average in the audio interface software (Audiomatica CLIO 12 Standard) installed on the host computer, based on the acoustic signals measured eight times.

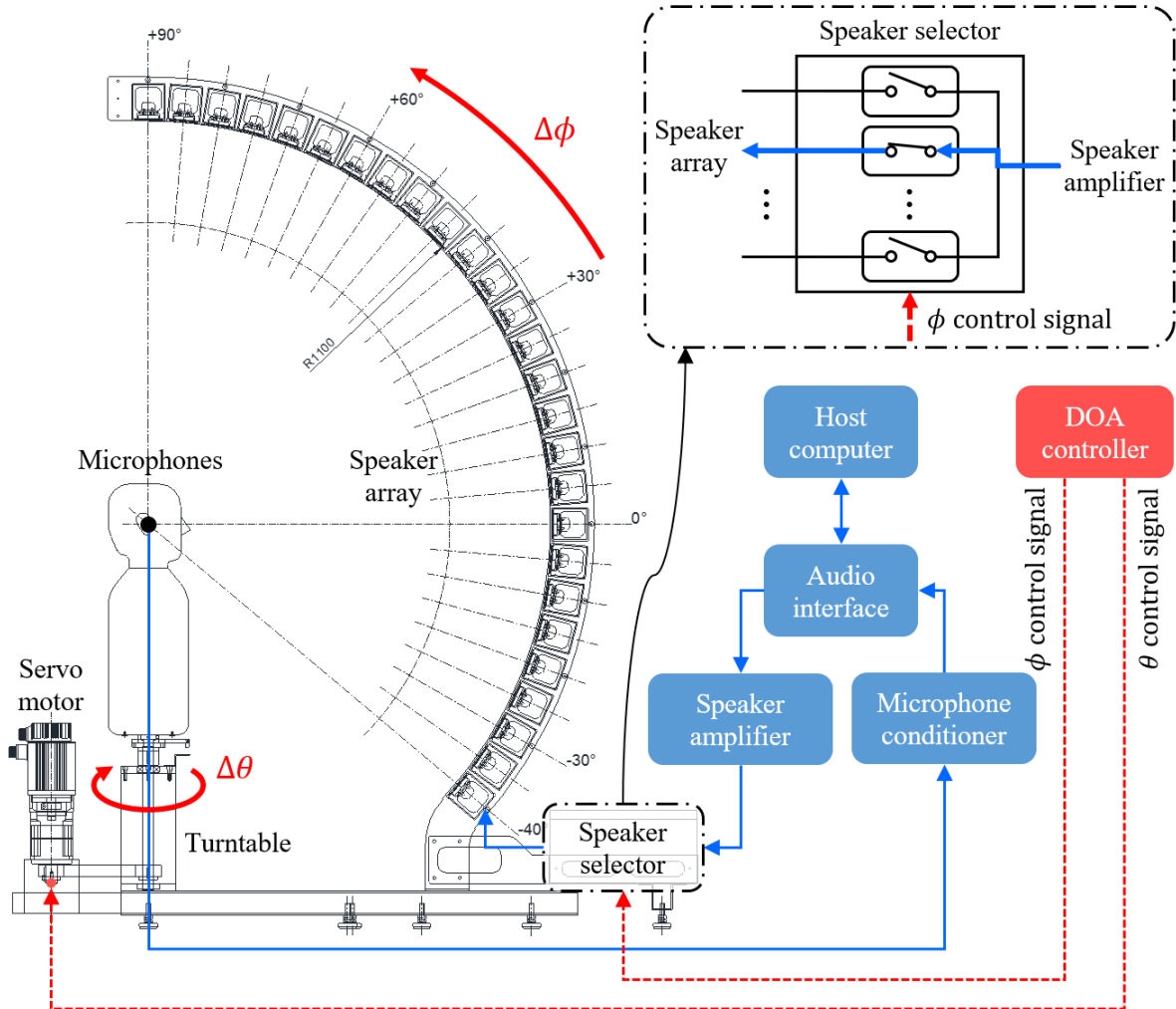


Fig. 3. Block diagram of the HRTF measurement system.

Among the measurement modules, the microphone conditioner is an acoustic measurement device, while the speaker amplifier is a commercial audio product. Thus, to verify the speaker amplifier, frequency response and total harmonic distortion (THD) were measured using an audio analyzer (Audio Precision) as follows. For the input voltage, $2.828 \text{ V}_{\text{rms}}$, $4.000 \text{ V}_{\text{rms}}$, and $4.899 \text{ V}_{\text{rms}}$ (power inputs of 1 W, 2 W, and 3 W) were applied based on the 8Ω speaker driver. As shown in Fig. 4, the magnitude response of the speaker amplifier is guaranteed to be flat from 20 Hz to 20 kHz, covering the frequency band of interest. In addition, the phase response is almost 0° from 10 Hz to 80 kHz, so there is no phase modulation for the input signal. Moreover, there is no harmonic distortion as the THD is almost 0% in the same frequency range. Therefore, the speaker amplifier is suitable for HRTF measurement.

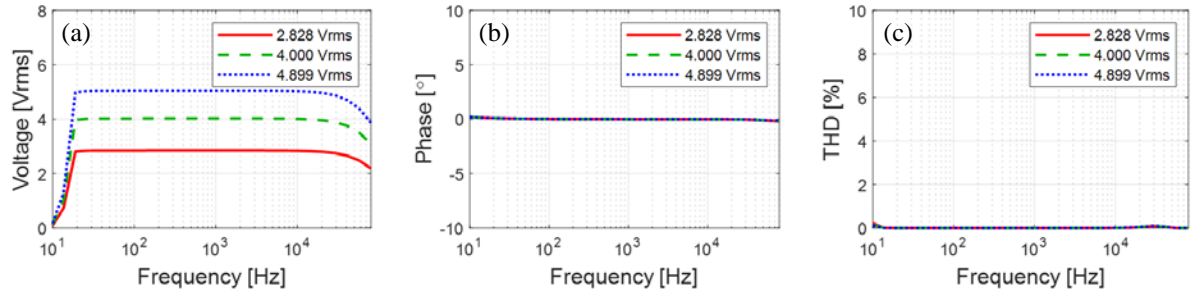


Fig. 4. Frequency responses of the speaker amplifier (YBA Heritage A200): (a) magnitude response; (b) phase response; (c) THD.

3.2. Electroacoustic based speaker module design

A full-range speaker driver (Peerless by Tympany PLS-P830986) was selected to reproduce the frequency band of interest (120 Hz to 20 kHz) with single sound source. Since the diameter of the speaker driver is 3 inches, it can be mounted on speaker modules arranged at 5° intervals in the speaker array. To simulate the frequency response of a speaker module using an equivalent acoustic circuit, the Thiele-Small parameters (TSPs) of the speaker driver were obtained using the delta mass method [46]. The delta mass method is a method of determining the electroacoustic parameters of a speaker driver through model curve fitting by referring to the electrical impedance curves of the speaker driver according to the presence or absence of additional mass on the diaphragm. As shown in Fig. 5, when 1.0 g of mass is attached to the diaphragm, it can be seen that the resonant frequency decreases due to the increase of the moving mass of the speaker driver.

Table 1 shows the obtained TSPs of the speaker driver. Resonance frequency F_0 appears as 101.221 Hz, enabling reproduction of the frequency band of interest under an infinite baffle condition.

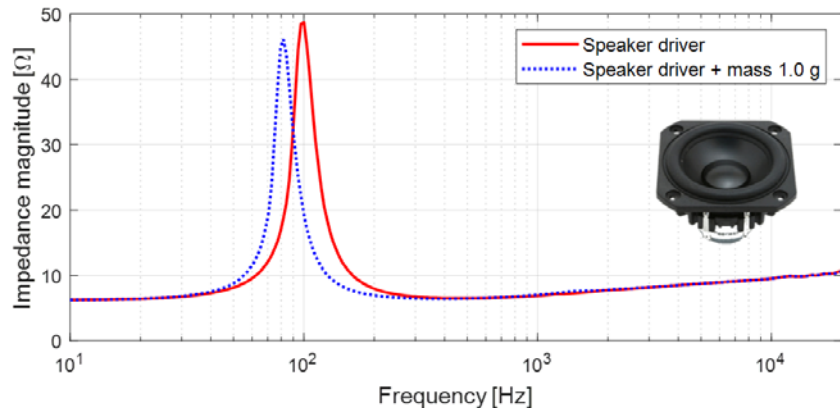


Fig. 5. Electrical impedance curves of the speaker driver (Peerless by Tympany PLS-P830986) to calculate Thiele-Small parameters (TSPs) by delta mass method.

Table 1

TSPs of the speaker driver to be used in the speaker module of the HRTF measurement system.

Parameter	Value	Description
R_{evc}	6.291 Ω	Voice coil resistance.
F_0	101.221 Hz	Resonance frequency.
S_d	0.002827 m^2	Equivalent diaphragm area.
K_{rm}	0.010251 Ω	Resistance constant of the motor impedance.
E_{rm}	0.503	High frequency slop of the motor resistance.
K_{xm}	0.040639 H	Reactance constant of the motor impedance.
E_{xm}	0.392	High frequency slop of the motor reactance.
V_{as}	1.255 ℓ	Equivalent acoustic volume.
C_{ms}	0.001106 m/N	Equivalent mechanical compliance.
M_{md}	2.150 g	Mechanical mass of the diaphragm without air load.
M_{ms}	2.236 g	Equivalent mechanical mass of the diaphragm with air load.
BL	3.265 Tm	Product of magnetic flux density and length of wire in the flux.
Q_{ms}	4.531	Measure of mechanical loss in the suspension.
Q_{es}	0.839	Measure of electrical loss in the voice coil.
Q_{ts}	0.708	Measure of total loss.
N_0	0.150 %	Conversion efficiency from electrical to acoustical energy.
SPL_0	83.778 dB	Sensitivity for half space radiation with 1 W input at 1 m.

In addition, the measure of total loss Q_{ts} is 0.708, indicating that the damping of the speaker driver is appropriate for low-frequency reproduction. Finally, SPL_0 is 83.778 dB, suggesting that the sensitivity of the speaker driver is high enough for acoustic measurement. A sealed speaker enclosure shifts the resonant frequency of a loudspeaker to a higher frequency because the air inside acts as an elastic support. As a result, the sealed speaker enclosure reduces the low-frequency band of a loudspeaker, and this tendency is exacerbated as the internal air volume decreases. Therefore, to design a speaker module that can reproduce the band of interest in the limited space, the frequency response of the sealed speaker module according to the internal air volume was simulated using the equivalent acoustic circuit shown in Fig. 6.

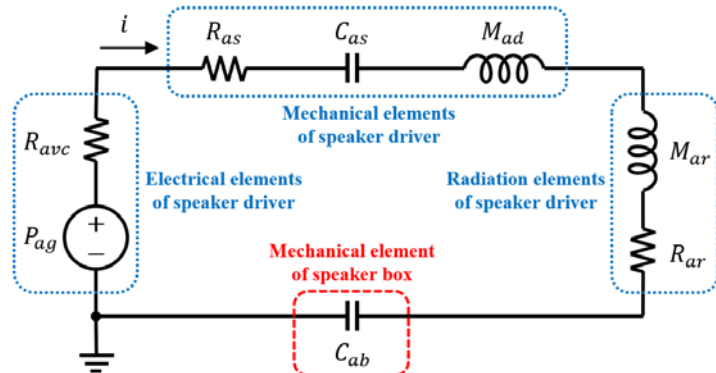


Fig. 6. Equivalent acoustic circuit of the sealed speaker module composed of a speaker drive and a speaker box.

In Fig. 6, the equivalent acoustic circuit of the sealed speaker module consists of two parts: the speaker driver and the speaker box. For the electrical elements of the speaker driver, voice coil current i , pressure generator P_{ag} , and voice coil resistance R_{avc} are expressed as [46]

$$i = V_{eg}/R_{evc}, \quad (6)$$

$$P_{ag} = BL \cdot i/S_d, \quad (7)$$

$$R_{avc} = (BL/S_d)^2/R_{evc}, \quad (8)$$

where V_{eg} is the input voltage of the speaker driver. The mechanical elements of the speaker driver consist of suspension resistance R_{as} , suspension compliance C_{as} , and diaphragm mass M_{ad} , and are defined as [46]

$$R_{as} = R_{ms}/S_d^2, \quad (9)$$

$$C_{as} = C_{ms} \cdot S_d^2, \quad (10)$$

$$M_{ad} = M_{md}/S_d^2, \quad (11)$$

where R_{ms} denotes the mechanical suspension resistance of the speaker driver. The radiation elements of the speaker driver are composed of radiation mass M_{ar} and radiation resistance R_{ar} , and are expressed as [42]

$$M_{ar}(\omega) = X_{ar}/\omega, \quad (12)$$

$$X_{ar}(ka) = (\rho_0 c/S_d)[H_1(2ka)/ka], \quad (13)$$

$$R_{ar}(ka) = (\rho_0 c/S_d)[1 - J_1(2ka)/ka], \quad (14)$$

where X_{ar} is the radiation reactance of the diaphragm, ω angular frequency, k wave number, a the radius of the diaphragm, and $\rho_0 c$ the characteristic impedance of air. In addition, $H_1()$ and $J_1()$ denote the first order Struve function and the first order Bessel function of the first kind, respectively. In Fig. 6, the speaker box consists of only the mechanical element, C_{ab} , and is defined as [42]

$$C_{ab} = S_d^2/k_{box}, \quad (15)$$

$$k_{box} = \rho_0 c^2 S_d^2 / V_{box}, \quad (16)$$

where k_{box} is the effective stiffness of the air inside the speaker box, ρ_0 the density of air, c the speed of sound, and V_{box} the internal air volume of the speaker box. Therefore, the total acoustic circuit impedance, $Z_{as}(\omega)$, and the volume velocity, $U_a(\omega)$, generated by the diaphragm are expressed as follows:

$$Z_{as}(\omega) = [R_{avc} + R_{as} + R_{ar}(\omega)] + j\omega[M_{ad} + M_{ar}(\omega)] + [1/j\omega C_{as} + 1/j\omega C_{ab}], \quad (17)$$

$$U_a(\omega) = P_{ag}/Z_{as}(\omega). \quad (18)$$

Finally, from Eq. (18), the speaker diaphragm excursion, $X(\omega)$, and the sound pressure along the acoustic axis, $p(\omega, r)$, can be obtained as [42]

$$X(\omega) = U_a(\omega)/j\omega S_d, \quad (19)$$

$$p(\omega, r) = U_a(\omega) \frac{2\rho_0 c}{S_d} \left| \sin \left[\frac{\omega}{2c} \left(\sqrt{r^2 + \frac{S_d}{\pi}} - r \right) \right] \right|, \quad (20)$$

where r is the microphone distance from the speaker diaphragm on the acoustic axis. Fig. 7 shows simulation results for the frequency responses of the speaker module. Simulation conditions were an input voltage of 2.828 V_{rms}, a microphone distance of 1 m from the speaker, and a speaker air volume of 800 cc. From Fig. 7(a), the maximum excursion of the speaker diaphragm occurs at 127 Hz and is expected to be less than 1.0 mm. As shown in Fig. 7(b), the volume velocity generated by the speaker diaphragm is expected to exceed 0.002 m³/s at 162 Hz. Fig. 7(c) shows the sound pressure in dB SPL

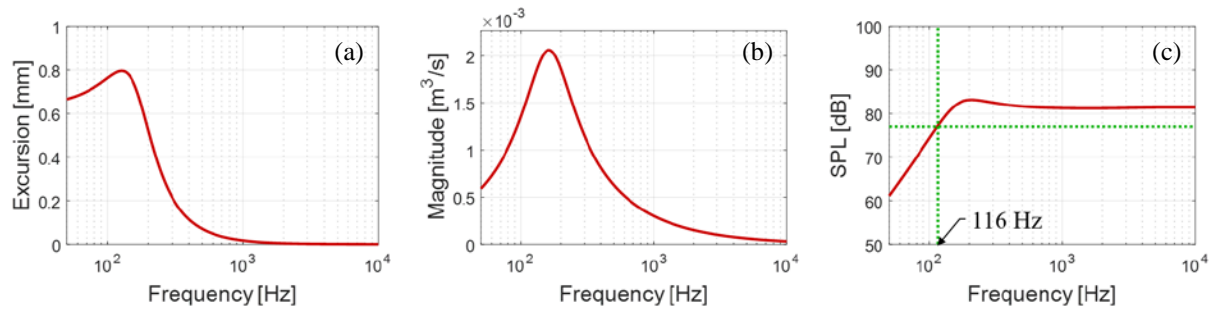


Fig. 7. Computed frequency responses of the sealed speaker module under the conditions of $V_{eg} = 2.828$ V_{rms}, $r = 1$ m, and $V_{box} = 800$ cc: (a) speaker diaphragm excursion; (b) volume velocity generated by the diaphragm; (c) sound pressure along the acoustic axis in dB SPL.

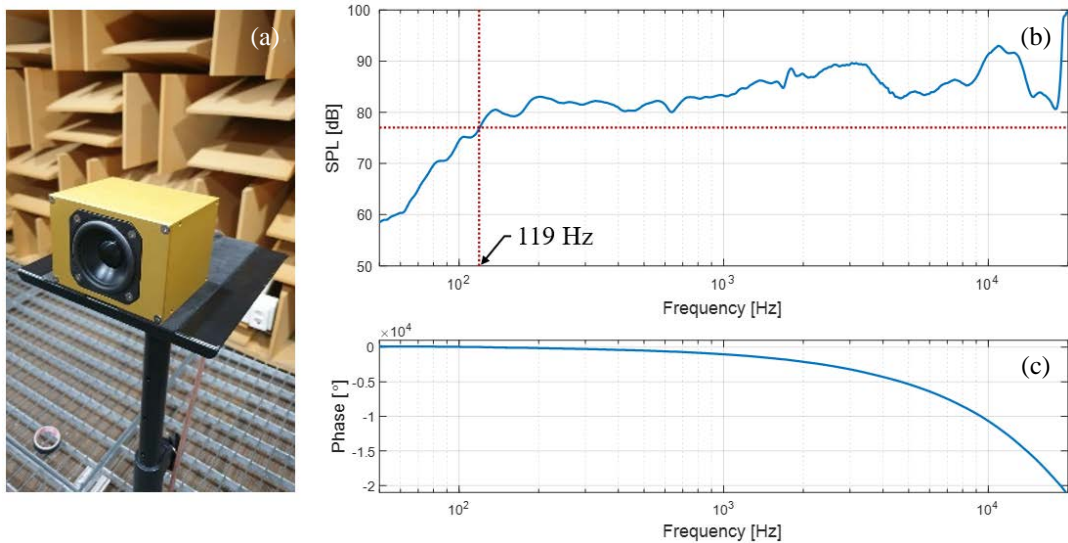


Fig. 8. Frequency responses of the speaker module measured at a microphone placed 1m in front of the speaker diaphragm when the input voltage is 2.828 V_{rms} (1 W for the 8 Ω speaker driver): (a) speaker module prototype; (b) magnitude response (1/12 octave bands); (c) unwrapped phase response.

at 1 m in front of the speaker diaphragm. The -6 dB roll-off frequency appears as 116 Hz, which is expected to sufficiently cover the frequency band of interest. Finally, a speaker module prototype was made based on the internal air volume of 800 cc as shown in Fig. 8(a).

To verify the performance of the speaker module prototype, the frequency response was measured 1 m in front when the input voltage was $2.828 \text{ V}_{\text{rms}}$. As shown in Fig. 8(b), the -6 dB roll-off frequency was found to be 119 Hz, which is almost consistent with the simulation result, and it was confirmed that the frequency band of interest (120 Hz \sim 20 kHz) was sufficiently reproduced. The deviation of the frequency response is the unique characteristic of the speaker driver and is mitigated when HRTFs are obtained by normalizing BTFs to OTFs later. Fig. 8(c) is the phase response of the speaker module prototype, showing a typical linear phase. Therefore, it can be expected that a sound wave reproduced by the speaker module will be radiated without distortion of the waveform.

4. Measurement of raw transfer functions

4.1. Binaural transfer function (BTF)

As shown in Fig. 9, a speaker array and measurement system were constructed based on the confirmed speaker module specifications. To measure BTFs, the positions of the dummy head and the speaker array were aligned so that the microphone of the dummy head faces the center of the speaker diaphragm at 0 degree of elevation. After installation in the anechoic chamber was completed, in order to minimize the effect of the reflection on the support of the measurement system, it was finished with sound-absorbing material as shown in Fig. 9(d). All measurements including OTFs as well as BTFs were performed with an input voltage of $2.828 \text{ V}_{\text{rms}}$ corresponding to 1 W for the 8Ω speaker driver.

Measurements of BTFs were performed for a total of 1,944 points, including 72 points of azimuth ($-180^\circ \sim +180^\circ$ with 5° resolution) and 27 points of elevation ($-40^\circ \sim +90^\circ$ with 5° resolution). Fig. 10 shows the results of BTFs for the horizontal plane ($\phi = 0^\circ$). Fig. 10(a1) and (a2) are BIRs, which are the time domain impulse responses of BTFs. The impulse response starts first when the sound source is in the ipsilateral 90° direction ($\theta = -90^\circ$ for the left or $\theta = +90^\circ$ for the right), and last when it is in the contralateral 90° direction ($\theta = +90^\circ$ for the left or $\theta = -90^\circ$ for the right). Fig. 10(b1) and (b2) show the magnitude responses of BTFs. It can be seen that the level of the mid and high frequency band of the contralateral BTFs was significantly lowered compared to the ipsilateral BTFs due to the head shadow effect. The peaks appearing around 20 kHz are due to the resonance frequency of the aluminum diaphragm of the speaker driver. Fig. 10(c1) and (c2) are the phase responses of BTFs. Also in the phase responses, it can be seen that the contralateral BTF phase of the mid and high frequency band changes rapidly due to the head shadow effect. Since the BTFs have not been post-processed yet, the reflection effect is noticeable in the time domain, and the speaker characteristics are revealed in the frequency

domain. Therefore, additional post-processing is required to estimate HRTFs from BTFs. In particular, the OTF including the transfer function of the entire measurement system is essential in the post-processing of BTFs. Detailed analysis will be done after obtaining HRTFs through post-processing including OTF normalization.



Fig. 9. BTF, $G_{L,R}$, measurement setup with the speaker array and the dummy head on the rotating turntable in the anechoic chamber at KAIST: (a) dummy head positioning; (b) speaker array positioning; (c) installation completed in the anechoic chamber; (d) floor finished with sound-absorbing material.

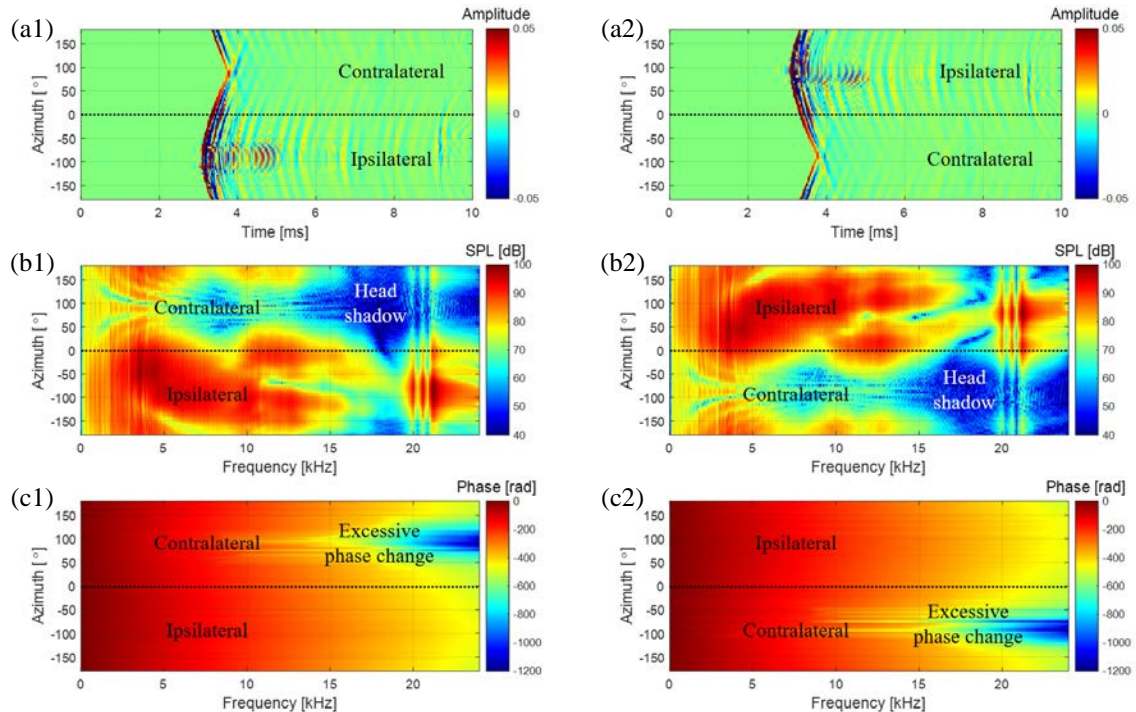


Fig. 10. BTFs, $G_{L,R}$, measurement results at $\phi = 0^\circ$: (a1) left BIRs; (a2) right BIRs; (b1) magnitude of left BTFs; (b2) magnitude of right BTFs; (c1) phase of left BTFs; (c2) phase of right BTFs.

4.2. Origin transfer function (OTF)

To obtain HRTFs, the transfer function of the measurement system included in the BTFs should be excluded and each origin of the BTFs should be moved to the center of the head, not the sound source. For this, an OTF, $G_0(\phi, f)$, which is the sound transfer function from a sound source to the center of the head, is required. Since OTF measurement is performed in the absence of a measurement target, only the transfer function of the measurement system is included. When measuring the OTF, the measurement system used for BTFs should be used as they are, so that the transfer function of the measurement system can be completely excluded from HRTF data later. Therefore, as shown in Fig. 11(a) and (b), the OTF measurement was performed using one of dummy head microphones. As shown in Fig. 11(c), the level difference between the left and right microphones was within ± 0.5 dB. Therefore, the right microphone was used for OTF measurements.

For all speaker modules, the OTF must be non-directional, but the microphone measuring it is directional. In some studies [21,29,39], the microphone was tilted 90° from the acoustic axis of the speaker as shown in Fig. 12(a). In other studies [31,32,40,41], the microphone was directed toward the acoustic axis as shown in Fig. 12(b). When a microphone is tilted 90°, there is no directivity in the circumferential direction of the microphone diaphragm, but directivity appears in its radial direction, so the high frequency level is lowered as shown in Fig. 12(c). Fig. 12(d) shows the level difference between the 90° off-axis and 0° on-axis microphones, and it can be seen that the level is reduced by about 11 dB or more up to 20 kHz. Therefore, normalizing the BTFs using the OTF measured with a 90° off-axis microphone will emphasize the high frequencies of the HRTFs by more than 11 dB. In addition, since various peaks and notches are distributed over the entire frequency band, estimating HRTFs using the OTF measured with a 90° off-axis microphone may give incorrect binaural localization cues which use

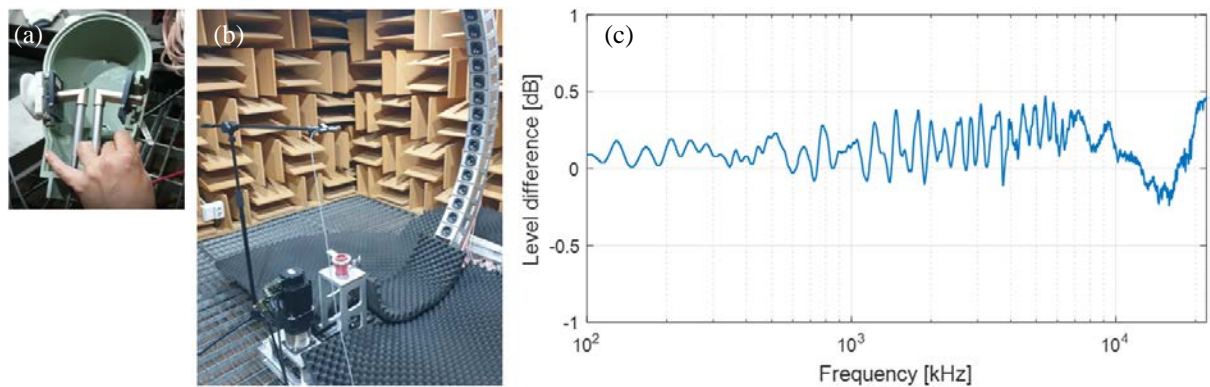


Fig. 11. Difference between the left and right microphones of the dummy head: (a) microphones inside the dummy head; (b) measurement setup with the speaker module at $\phi = 0^\circ$ turned on; (c) level difference between the left and right microphones.

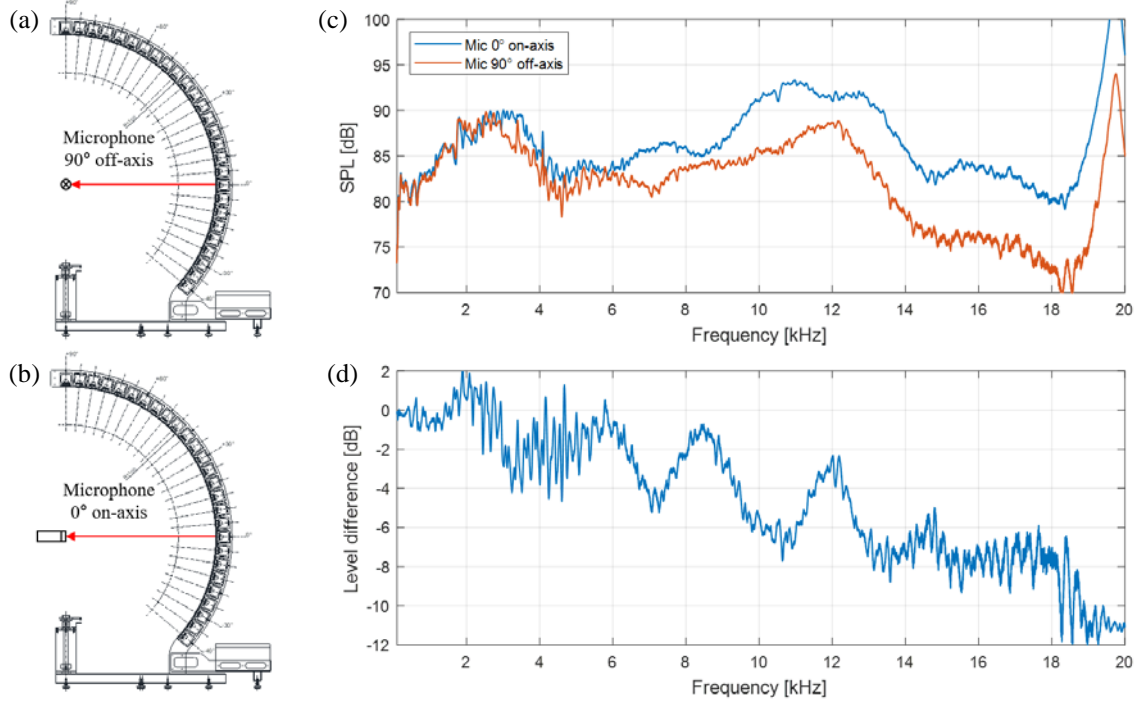


Fig. 12. Difference between two representative OTF, G_0 , measurements: (a) measurement setup with 90° off-axis microphone; (b) measurement setup with 0° on-axis microphone; (c) frequency responses of OTF measured with 0° on-axis microphone and 90° off-axis microphone respectively; (d) level difference between 90° off-axis and 0° on-axis OTFs.

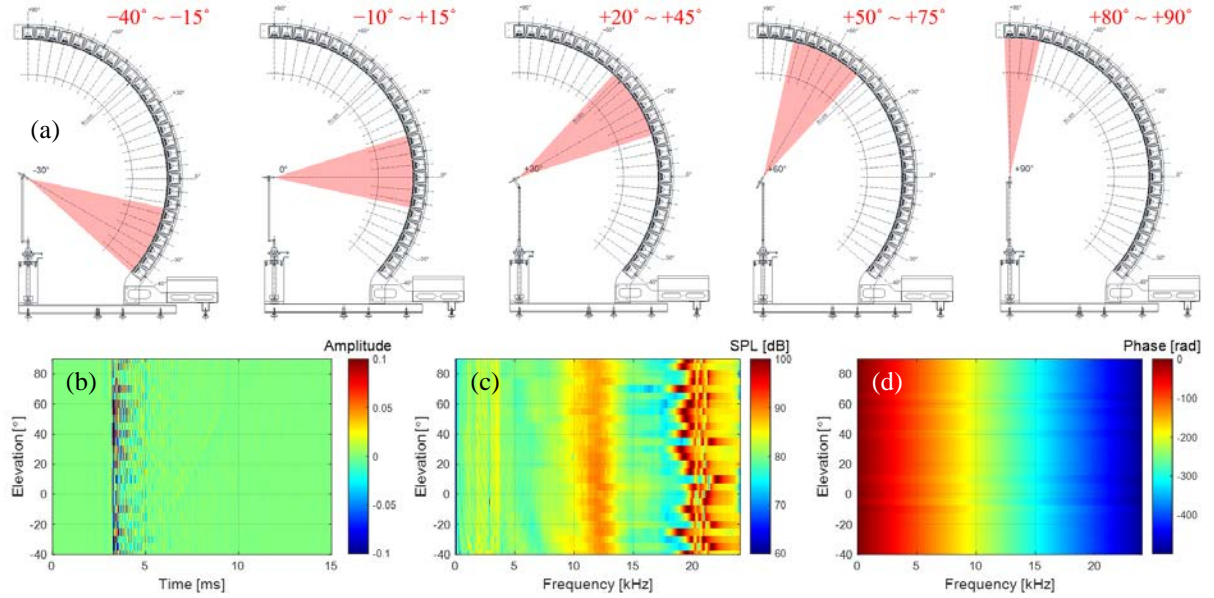


Fig. 13. OTFs, G_0 , measurement setup and results: (a) divided measurement to obtain the omnidirectional OTF; (b) OIRs; (c) magnitude of OTFs; (d) phase of OTFs.

peaks and notches of HRTF. As shown in Fig. 12(b), when measuring with the microphone facing the acoustic axis of each speaker module, the omnidirectional OTF can be obtained, but it is cumbersome to redirect the direction of the microphone every time. However, most microphones have an angular section close to omnidirectional. As a result of the directivity measurement of the dummy head microphone, it was confirmed that the microphone was omnidirectional with an error of ± 0.5 dB in an angular range within $\pm 15^\circ$.

In this measurement, as shown in Fig. 13(a), the entire measurement section of the speaker array was divided into five sections in consideration of the microphone's omnidirectional range (maximum 30°). In addition, the microphone was directed to the elevation angles of -30° , 0° , $+30^\circ$, $+60^\circ$, $+90^\circ$, respectively, and the OTF for each speaker module in the corresponding section was measured. Fig. 13(b) shows the impulse responses of OTFs according to the elevation angle. At about 3.2 ms, which is the time it takes for the sound wave to propagate 1.1 m, the maximum peaks of the impulse responses are equally represented. Fig. 13(c) is the magnitude responses of OTFs. The peaks around 12 kHz and 20 kHz are intrinsic frequency characteristics of the applied speaker drivers. Fig. 13(d) shows the phase responses of the BTF, showing the linear phase. In this way, the divided measurement method considering the omnidirectional range of the on-axis microphone makes it possible to obtain the omnidirectional OTF while minimizing the number of microphone settings.

4.3. Time window setting

The sample size of the measured BIR and OIR is 4,096, which corresponds to about 85.3 ms when the sampling rate is 48 kHz. Since the essential information of the measured impulse responses is limited to several ms, it is necessary to remove unnecessary sections in order to minimize the storage space of the HRTF database. In this measurement, the start and end points of the time window were set in consideration of the propagation delay and reflective ripples of each impulse response and then applied to each BIR and OIR. The start point of the time window should be set based on the most preceding impulse response to preserve all BIR and OIR information. Therefore, the start point was set based on the maximum sample positions of left ipsilateral 90° BIR, $g_L(-90,0,t)$, and right ipsilateral 90° BIR, $g_R(+90,0,t)$. As shown in Fig. 14, the maximum sample of both $g_L(-90,0,t)$ and $g_R(+90,0,t)$ appear at 3.1 ms. Due to some measurement error in signal processing, there may be small ripples located before the maximum sample in the measured impulse response [5]. Therefore, to include the ripples, the start point should be set before the maximum sample. In this measurement, a point 1 ms before the maximum sample of ipsilateral 90° BIRs was set as the start point of the time window.

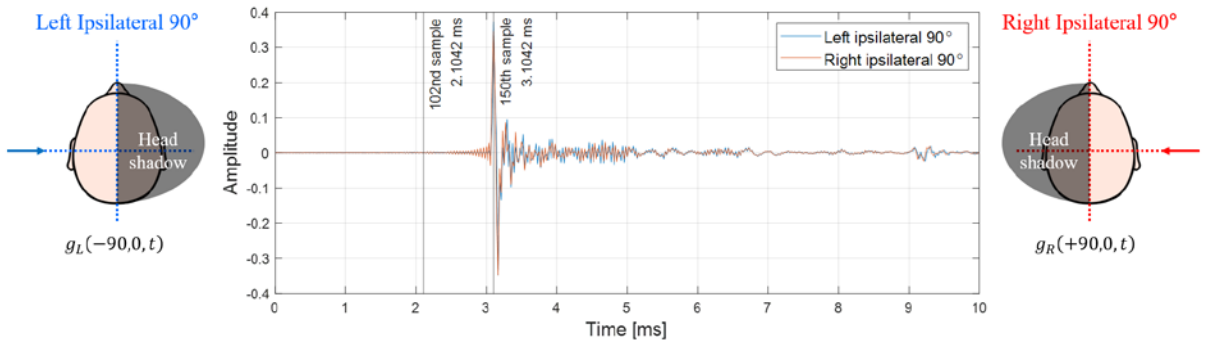


Fig. 14. BIRs, $g_{L,R}$, of the ipsilateral 90° directions for setting the start point of the time window.

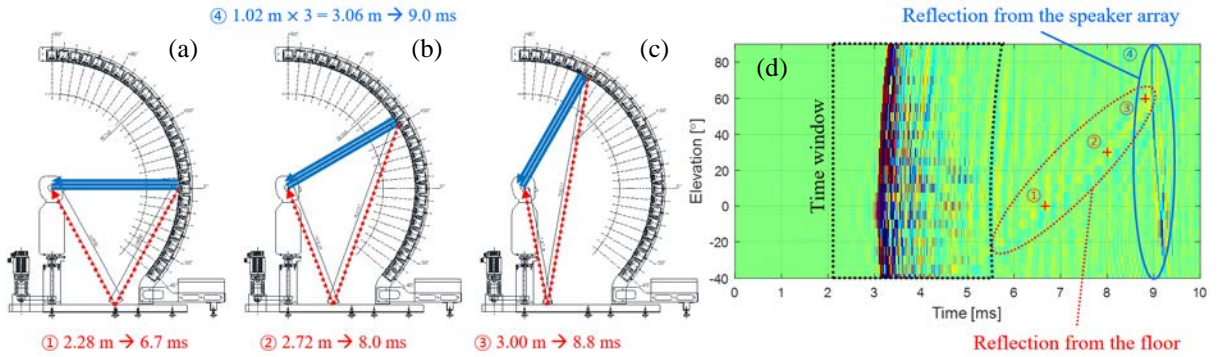


Fig. 15. Illustrations for setting the end point of the time window: (a) reflections when the speaker module at $\phi = 0^\circ$ is turned on; (b) reflections when the speaker module at $\phi = 30^\circ$ is turned on; (c) reflections when the speaker module at $\phi = 60^\circ$ is turned on; (d) right ipsilateral 90° BIRs, $g_R(+90, \phi, t)$, with the time window and reflections from the floor and the speaker array.

The end point of the time window is set to eliminate reflective ripples in the measured impulse response. Even if BIR and OIR are measured in an anechoic chamber, reflections from the measurement system are unavoidable. As shown in Fig. 15, the main reflections attributed to the measurement system are speaker array reflections and floor support reflections. Since all speaker modules are arranged equidistant from the origin at the head center, the arrival time from the speaker array reflections is almost constant regardless of the elevation angle of the speaker module that reproduces sound. On the other hand, as the elevation angle of the speaker module is lowered, the arrival time of the floor support reflection becomes gradually shorter because the reflection path is shortened. Therefore, the bottom reflection of the lowest elevation speaker module arrives first. Even if the measurement system is finished with a sound-absorbing material to mitigate the reflection of the floor support, the low-frequency components of the reflected wave remain as shown in Fig. 15(d). Therefore, all BIRs and OIRs need to be preprocessed to keep only the key information in time window where there is no

reflection. In this measurement, the first zero-crossing sample after more than 2.5 ms (120 samples) after the max sample of each impulse response was set as the end point of the time window not to have reflections. Each BIR, $g_{L,R}(\theta, \phi, t)$, and OIR, $g_0(\phi, t)$, cut out by the time window was zero-padded to 512 samples for a resolution of 93.75 Hz.

5. Derivation of HRTFs

5.1. Compensation for non-causality of ipsilateral HRIR

The post-processed BIRs, $g_{L,R}(\theta, \phi, t)$, and OIRs, $g_0(\phi, t)$, are converted into BTFs and OTFs through the fast Fourier transform (FFT), respectively. HRTFs, $H_{L,R}(\theta, \phi, f)$, are obtained by complex division of BTFs, $G_{L,R}(\theta, \phi, f)$, by OTFs, $G_0(\phi, f)$, as written in Eq. (5). Since each HRTF consists of 512 complex numbers, when saved as a data file, 512 real numbers and 512 imaginary numbers are stored in two lines. Furthermore, when a pair of left and right HRTFs are stored together for each direction, a total of four lines are saved per direction. In general, to minimize the storage space of the database, HRTFs, $H_{L,R}(\theta, \phi, f)$, in frequency domain are converted into HRIRs, $h_{L,R}(\theta, \phi, t)$, in time domain through inverse fast Fourier transform (IFFT).

As shown in Fig. 16, ipsilateral HRTF is a kind of non-causal filter because the sound pressure P_R of the ipsilateral ear arrives earlier than the sound pressure P_0 at the head center. On the other hand, since the sound pressure P_L of the contralateral ear arrives later than the sound pressure P_0 of the head center, the contralateral HRTF is a causal filter. Due to the circularity characteristic of the discrete Fourier transform, the maximum sample preceding 0 seconds of the non-causal filter appears later in the impulse response sequence as shown in Fig. 16(a1). Therefore, additional post-processing is needed to compensate for the discontinuity of ipsilateral HRIRs.

In Fig. 16, the difference of the arrival times between sound pressures P_0 and P_R has maximum value when the azimuth angle is 90° in the horizontal plane, which can be obtained as follows:

$$\tau_{max} = l/c, \quad (21)$$

where l is radius of the head and c is the speed of sound in air. In this measurement, to compensate for the non-causality of ipsilateral HRIRs, all HRIRs were circular shifted by at least τ_{max} as follows:

$$h_{L,R}(\theta, \phi, n) = \tilde{h}_{L,R}(\theta, \phi, \langle n - m \rangle_N) \quad (22)$$

with $0 \leq n \leq N - 1$; $m > \tau_{max} F_s$,

where $\tilde{h}_{L,R}$ is a raw HRIR, n time index, m time delay index, N length of a HRIR (512 samples), and F_s sampling frequency (48 kHz). In addition, $\langle n - m \rangle_N$ denotes the circular shift operation. Through this compensation in Eq. (22), the maximum peak of the ipsilateral HRIR appears in the first half of the impulse response sequence as shown in Fig. 16(a2).

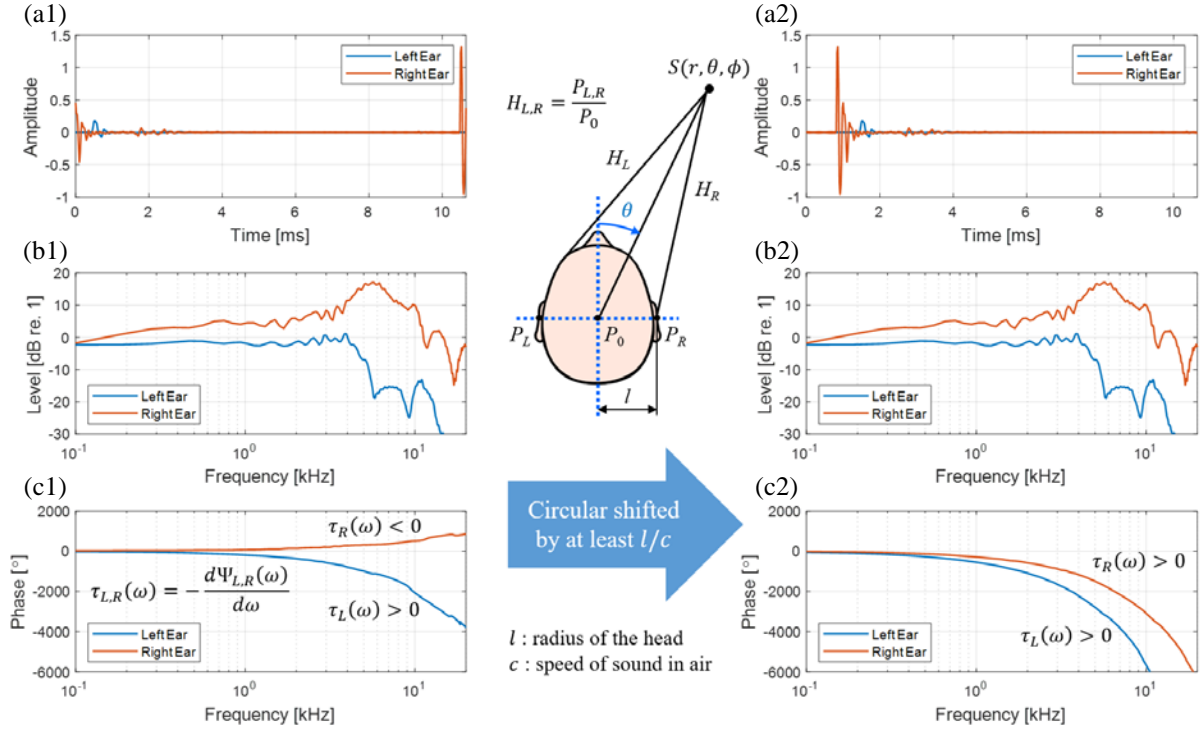


Fig. 16. Non-causality issue of ipsilateral HRIRs and compensation for the non-causality: (a1) non-causal HRIRs; (a2) causal HRIRs; (b1) non-causal HRTF magnitude responses; (b2) causal HRTF magnitude responses; (c1) non-causal HRTF phase responses; (c2) causal HRTF phase responses.

Comparing Fig. 16(b1) and (b2), the magnitude responses do not differ before and after the non-causality compensation. However, when comparing Fig. 16(c1) and (c2), both the left and right time delays (τ_L and τ_R) became positive after the non-causality compensation, confirming that the causality of HRIRs was secured. A pair of left and right HRIRs for each direction was saved as a text file consisting of two columns of 512 signed numbers. Finally, the HRTF database was constructed with a total of 1,944 HRIR text files (72 directions in azimuth \times 27 directions in elevation).

5.2. HRTF response according to azimuth and elevation

The time and frequency domain characteristics of the derived HRTFs were presented as contour maps for each major azimuth and elevation angle. Fig. 17–19 show left and right HRTF pairs as impulse responses, magnitude responses in dB scale, and phase responses in radian for the entire elevation range when the azimuth angles are 0° , 45° , and 90° , respectively.

As shown in Fig. 17 (a1) and (a2), the essential part of the HRIRs, which reflects the complex interactions between a sound source and the torso, head, and pinna, lasts about 1.0 ms. In addition, when the azimuth angle of a sound source is 0° , it can be seen that there is almost no time difference between

the left and right HRIRs regardless of the elevation angle. On the other hand, when the azimuth of a sound source is 45° , the sound wave reaches the right ear first. Thus, the time delay of the right HRIRs is shorter than that of the left as shown in Fig. 18(a1) and (a2). The arrival time difference between the left and right HRIRs is maximized in the horizontal plane ($\phi = 0^\circ$) when the azimuth of a sound source is 90° as shown in Fig. 19(a1) and (a2). The reason is that when the azimuth is 90° , the transmission path to the right ear is the shortest, while that to the left ear is the longest. When a sound source is on the left ($\theta < 0^\circ$), it appears in the form of left-right symmetry with the case on the right sound source ($\theta > 0^\circ$). The quantitative analysis of ITD for left and right HRIR pairs is covered in Section 6.1.

As shown in Fig. 17(b1) and (b2), at frequencies below 500 Hz, the level of HRTF approaches 0 dB regardless of frequency, since the scattering effect of the head is almost negligible. As frequency increases, the levels of HRTFs vary with frequency and elevation angle in a complex manner. This complexity is due to the overall filtering effects of the torso, head, and pinna. The apparent peak at 4 kHz is constant regardless of the elevation angle, while the notch at 9 kHz shifts to a higher frequency as the elevation angle increases. The relative positions of the HRTF peaks and notches serve as the localization cue of elevation and are discussed in detail in Section 6.3. When the azimuth angle is 0° , there is no significant difference in the left and right HRTF levels.

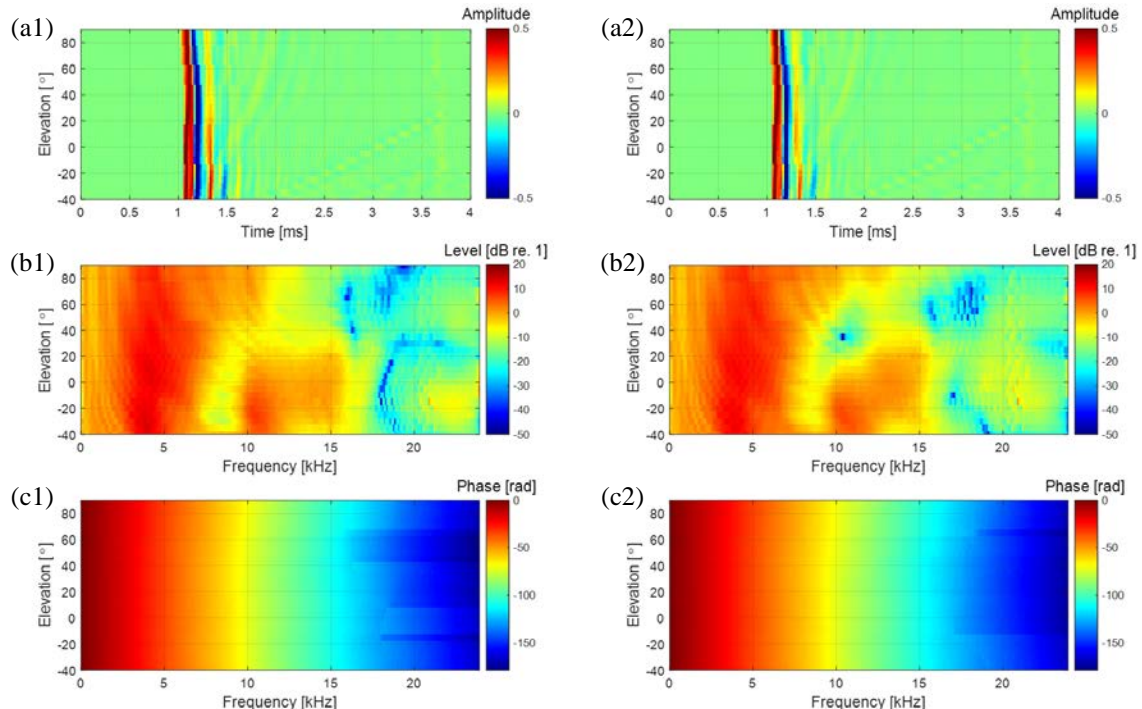


Fig. 17. HRTFs at $\theta = 0^\circ$, $H_{L,R}(0, \phi, f)$: (a1) left HRIRs; (a2) right HRIRs; (b1) magnitude of left HRTFs; (b2) magnitude of right HRTFs; (c1) phase of left HRTFs; (c2) phase of right HRTFs.

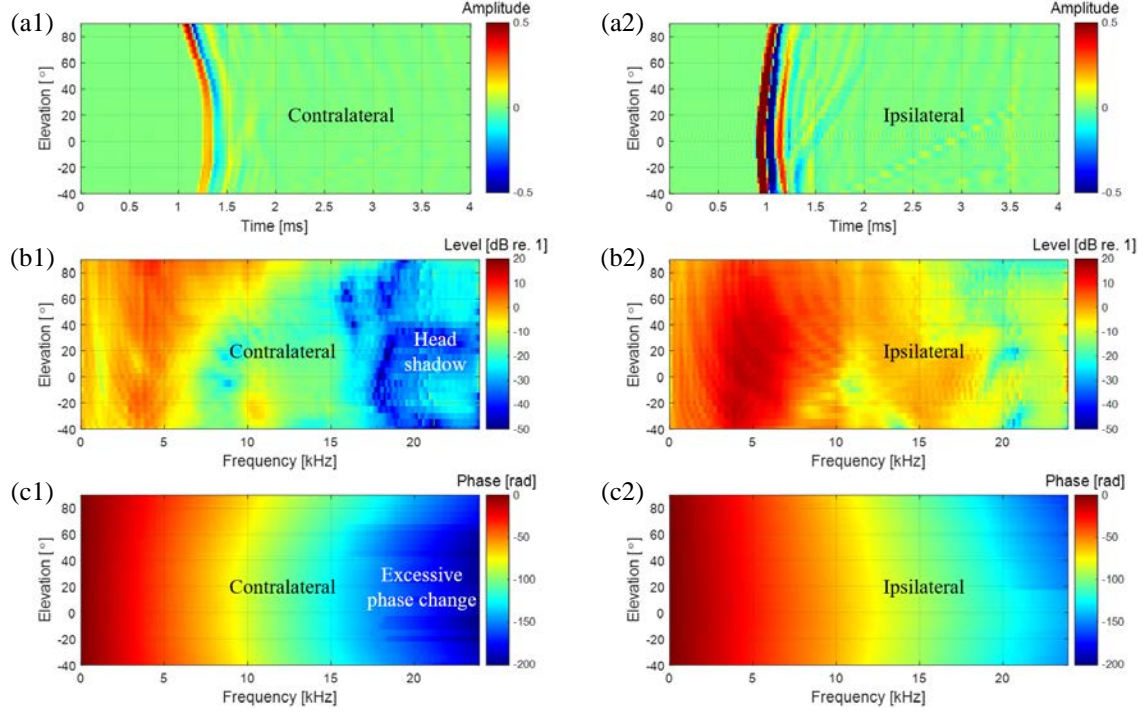


Fig. 18. HRTFs at $\theta = 45^\circ$, $H_{L,R}(45, \phi, f)$: (a1) left HRIRs; (a2) right HRIRs; (b1) magnitude of left HRTFs; (b2) magnitude of right HRTFs; (c1) phase of left HRTFs; (c2) phase of right HRTFs.

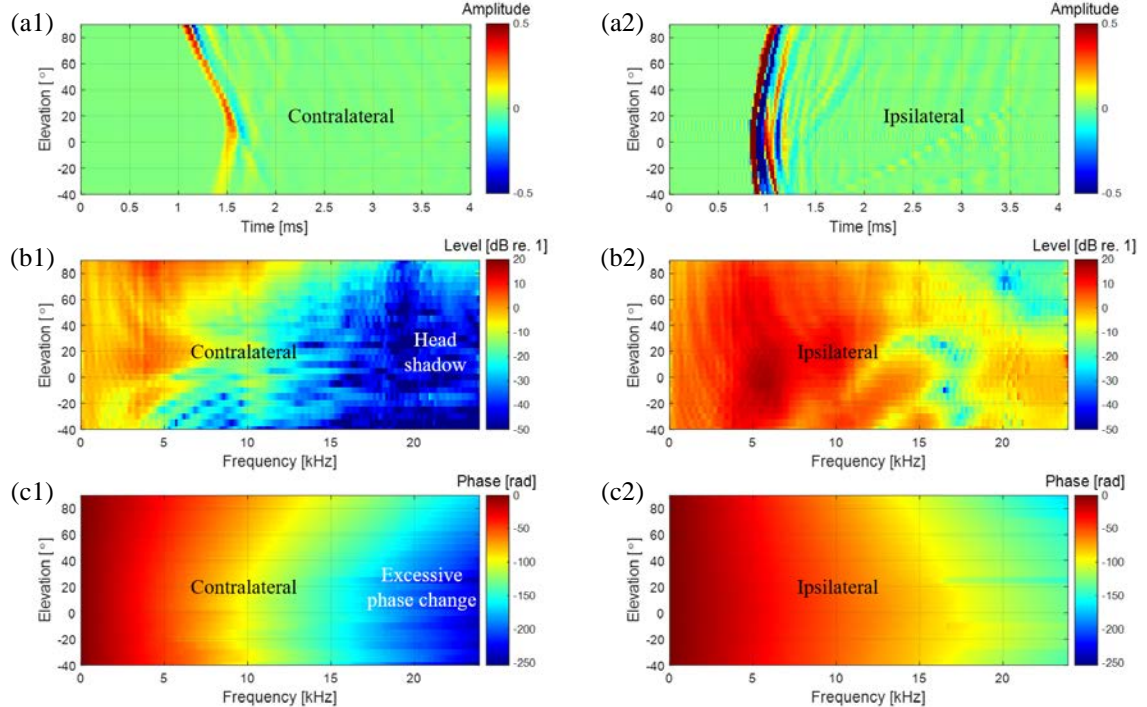


Fig. 19. HRTFs at $\theta = 90^\circ$, $H_{L,R}(90, \phi, f)$: (a1) left HRIRs; (a2) right HRIRs; (b1) magnitude of left HRTFs; (b2) magnitude of right HRTFs; (c1) phase of left HRTFs; (c2) phase of right HRTFs.

As shown in Fig. 18(b1) and (b2), when the azimuth of a sound source is 45° , a level difference appears between the left and right HRTFs. Above 4 kHz, the contralateral HRTF levels are noticeably attenuated due to the low-pass filtering effect of the head shadow. The ipsilateral HRTF levels increase to some extent, and some notches appear. This is due to the reflection effect of the head on ipsilateral incidence at high frequencies, which increases the pressure on the ipsilateral sound source. This phenomenon is maximized when a sound source is in the ipsilateral 90° direction as displayed in Fig. 19(b1) and (b2). The quantitative ILD analysis of left and right HRTF pairs is detailed in Section 6.2.

As shown in Fig. 17(c1) and (c2), when the azimuth is 0° , the phase change is close to a linear phase, and the phase patterns of the left and right HRTFs are almost the same. However, when the azimuth angle is 45° , an excessive phase change appears at high frequencies of the contralateral HRTF as presented in Fig. 18(c1) and (c2). This is another result of the head shadow effect reflected in the phase. The phase pattern of high frequencies changes most rapidly when a sound source is in the contralateral 90° direction as shown in Fig. 19(c1) and (c2).

Fig. 20–22 show left and right HRTF pairs as impulse responses, magnitude responses in dB scale, and phase responses in radian for the entire azimuth range when the elevation angles are 0° , 60° , and 90° , respectively. Looking at Fig. 20(a1) and (a2), when a sound source is in the ipsilateral direction,

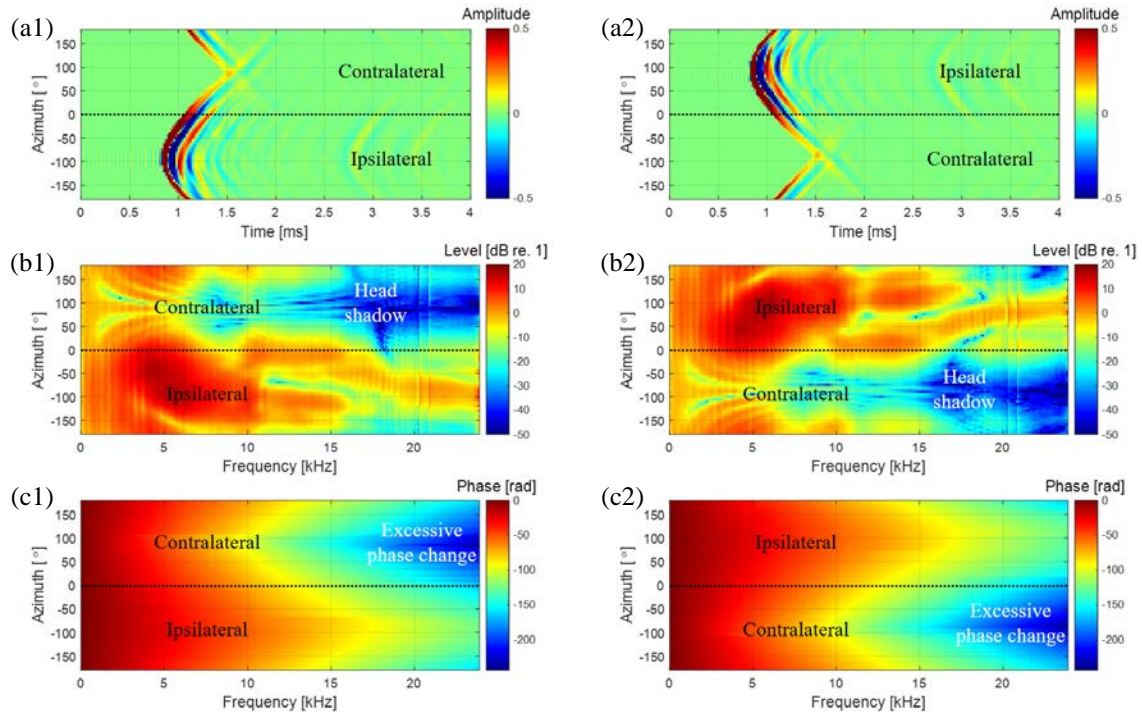


Fig. 20. HRTFs at $\phi = 0^\circ$, $H_{L,R}(\theta, 0, f)$: (a1) left HRIRs; (a2) right HRIRs; (b1) magnitude of left HRTFs; (b2) magnitude of right HRTFs; (c1) phase of left HRTFs; (c2) phase of right HRTFs.

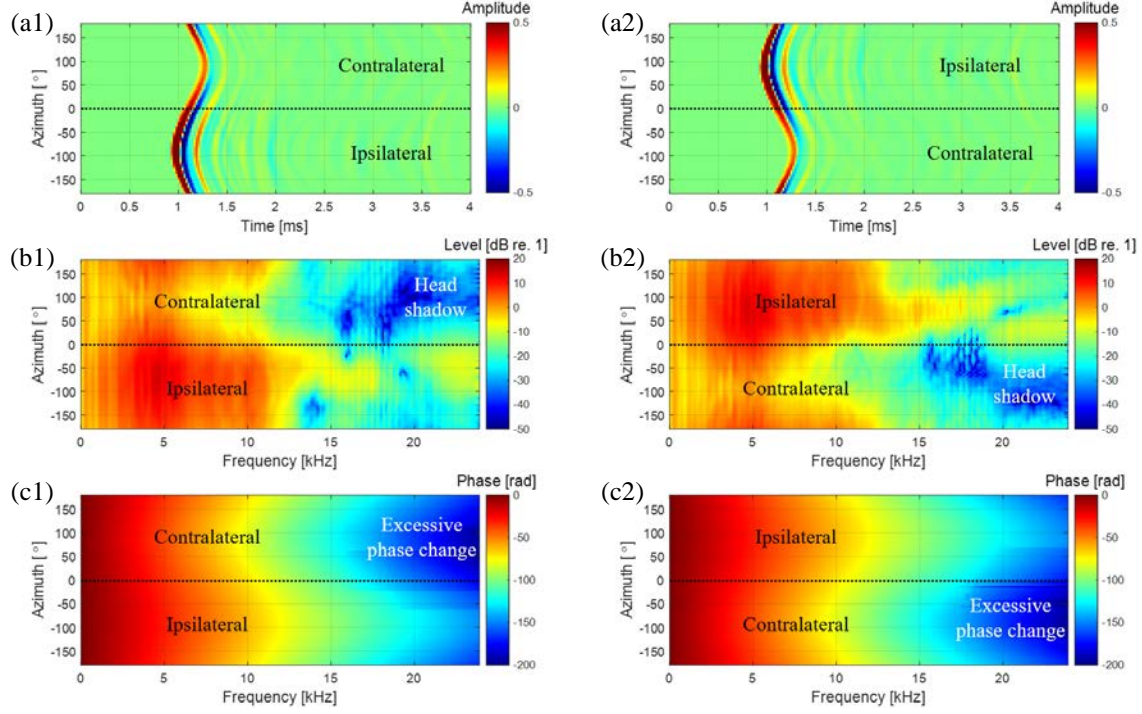


Fig. 21. HRTFs at $\phi = 60^\circ$, $H_{L,R}(\theta, 60, f)$: (a1) left HRIRs; (a2) right HRIRs; (b1) magnitude of left HRTFs; (b2) magnitude of right HRTFs; (c1) phase of left HRTFs; (c2) phase of right HRTFs.

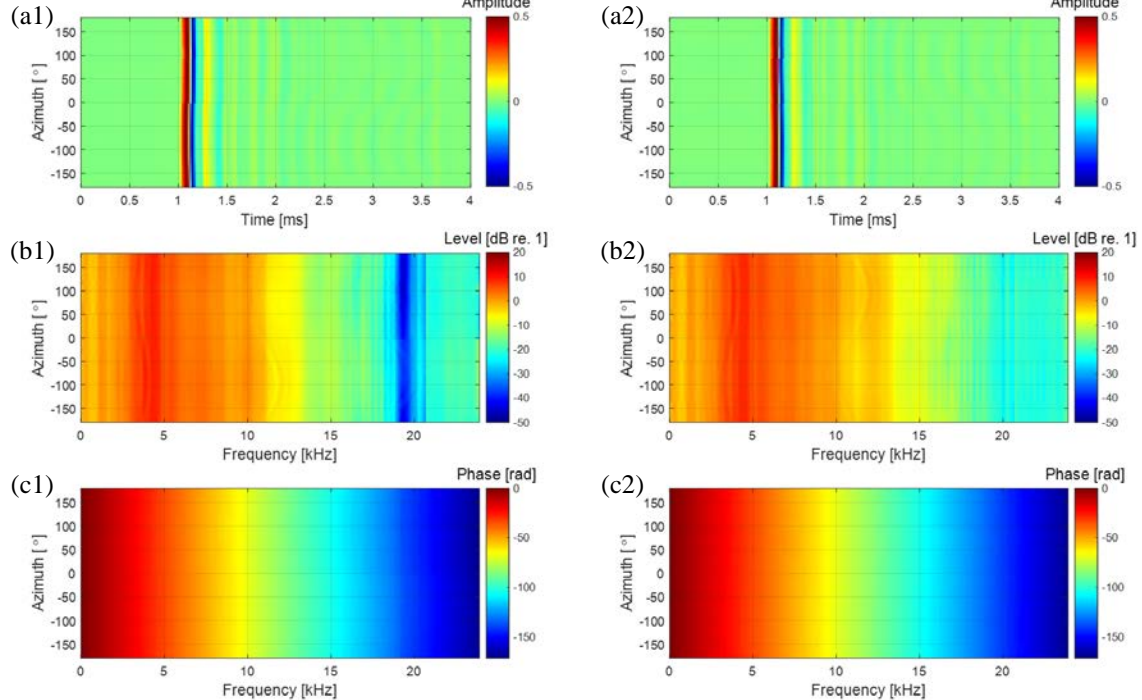


Fig. 22. HRTFs at $\phi = 90^\circ$, $H_{L,R}(\theta, 90, f)$: (a1) left HRIRs; (a2) right HRIRs; (b1) magnitude of left HRTFs; (b2) magnitude of right HRTFs; (c1) phase of left HRTFs; (c2) phase of right HRTFs.

$\theta = -90^\circ$ in Fig. 20(a1) or $\theta = +90^\circ$ in Fig. 20(a2), in the horizontal plane ($\phi = 0^\circ$), the time delay of the ipsilateral HRIR is the shortest and there are many ripples after the maximum peak. On the other hand, when a sound source is in the contralateral direction, $\theta = +90^\circ$ in Fig. 20(a1) or $\theta = -90^\circ$ in Fig. 20(a2), it can be seen that the time delay of the contralateral HRIR is the longest and there are almost no ripples. This is due to the low-pass filtering effect of the head shadow. As shown in Fig. 20(b1) and (b2), when a sound source is located contralateral to the related ear, for example, at an azimuth of 90° for the left ear, the HRTF level decreases noticeably from 4 kHz because of the head shadow effect. As presented in Fig. 20(c1) and (c2), the phase change in the ipsilateral 90° direction is gentle, while the phase change in the contralateral 90° direction is steep. In Fig. 21 and 22, with increasing elevation, the azimuth-dependent variations in HRIRs, magnitude, and phase responses, decrease and smoothen.

6. Localization cues from HRTFs

Based on the measured HRTF database, various HRTF features can be analyzed to obtain useful information about the localization cues encoded in HRTFs. Psychoacoustic studies have shown that binaural sound localization cues for a single sound source include ITD, ILD, and SCs [36]. Thus, ITD, ILD, and SCs were derived from the measured HRTF database to analyze binaural sound localization cues in the HRTF. In addition, the directivity of the left and right HRTF pairs in the horizontal plane was obtained by defining the HPD and representing it as directional beam patterns. By analyzing ITD, ILD, SCs, and HPD in the measured HRTF, we examined whether binaural sound localization cues are accurately identified by the presented methods. The effects of speaker module bandwidth and time window interval on sound localization cues are clear, and thus they were not investigated further. Instead, the effects of OTF measurement method and non-causality compensation on sound localization cues were focused on.

6.1. Interaural time difference (ITD)

ITD refers to the time difference of sound waves reaching the left and right ears and plays an important role in BSSL. In the median plane, ITD is nearly zero because the paths from a sound source to both ears are approximately equal in length. However, if the sound source is off the median plane, the path lengths to both ears become different, so the ITD results in a non-zero value. ITD can be estimated from a pair of left and right HRTFs. As stated in Ref. [5], interaural phase delay difference (ITD_p) is a dominant localization cue below 1.5 kHz, whereas interaural envelope delay difference (ITD_e) is useful for BSSL above 1.5 kHz. However, ITD_p is complicated due to its frequency dependence, and ITD_e is not directly analyzed because of its dependence on the signal type [5]. Hence, ITD was estimated in this paper based on the similarity between left and right HRIRs by using cross-

correlation method. The normalized cross-correlation function of a pair of left and right HRIRs is calculated as follows:

$$ITD(\theta, \phi) = \operatorname{argmax}_{\tau} \frac{\int_{-\infty}^{+\infty} h_L(\theta, \phi, t) h_R(\theta, \phi, t - \tau) dt}{\sqrt{\left[\int_{-\infty}^{+\infty} h_L^2(\theta, \phi, t) dt \right] \left[\int_{-\infty}^{+\infty} h_R^2(\theta, \phi, t) dt \right]}} \quad (23)$$

with $|\tau| \leq 1000 \mu\text{s}$,

where τ is time delay. Before the calculation of Eq. (23), a pair of HRIRs is subjected to low-pass filtering with a cutoff frequency of 1.5 kHz. The reason is that above 1.5 kHz, when the head dimension is larger than the wavelength, the left and right phase difference exceeds 2π , resulting in ambiguous ITD. To improve the ITD resolution, the filtered HRIRs are upsampled four times to improve the time resolution to about $5.2 \mu\text{s}$.

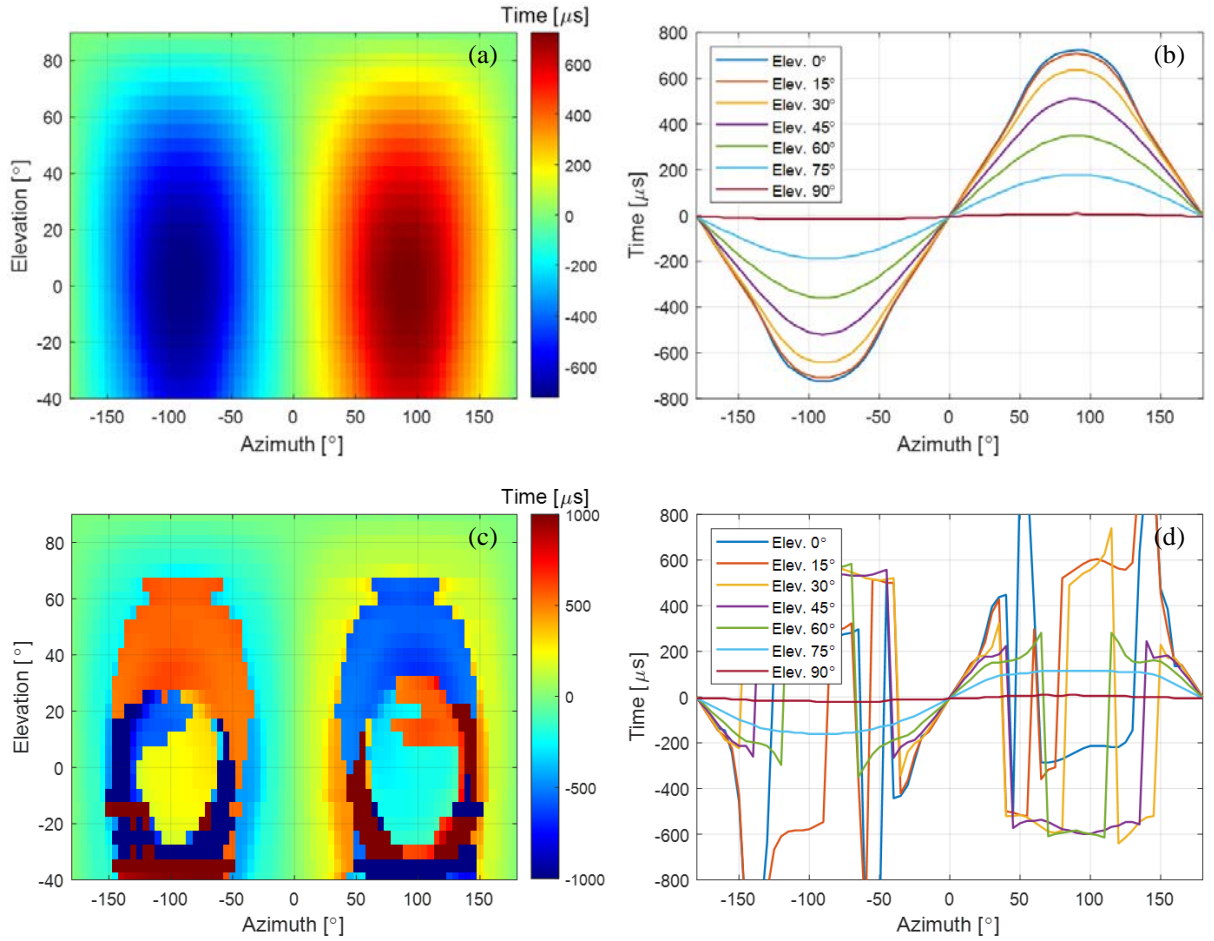


Fig. 23. ITDs that change with azimuth and elevation: (a) ITD contour map of causal HRTF; (b) ITD plots of causal HRTF for seven elevation angles; (c) ITD contour map of non-causal HRTF; (d) ITD plots of non-causal HRTF for seven elevation angles.

Fig. 23(a) and (b) show the ITD contour map and its cutting plots with azimuths from -180° to $+180^\circ$ from the measured HRTF database, respectively. In Fig. 23(a) and (b), the ITDs are zero at 0° and 180° in azimuth and increases gradually as a sound source deviates from the median plane ($\theta = 0^\circ$). As the sound source approaches lateral 90° directions ($\theta = -90^\circ$ or $+90^\circ$), the absolute value of ITD increases and reaches its maximum near -90° and $+90^\circ$ in azimuth. Around the lateral 90° directions, a small change in ITD corresponds to a large change in azimuth angle. Compared to the results for other elevations, the extent of ITD variation is maximum in the horizontal plane ($\phi = 0^\circ$). As the source moves out of the horizontal plane, the range of ITD variations decreases.

Fig. 23(c) and (d) show the ITD contour map and its cutting plots obtained from HRTF database without non-causality compensation. Since ipsilateral HRIR is a non-causal filter, its maximum peak appears later in the HRIR sequence. On the other hand, since contralateral HRIR is a causal filter, its maximum peak appears early in the HRIR sequence. Therefore, when the ITD is obtained from the non-causal HRIR pair, a sharp discontinuity occurs compared to that obtained from the causal HRIR pair. If a sound source is located in the front (near 0° azimuth), rear (near 180° azimuth), and top (elevation over 70°) of the head, the sound wave reaches the head center before both ears, so the ITD discontinuity due to non-causality disappear. On the other hand, the direction (0° on-axis or 90° off-axis) of the microphone for OTF measurement does not affect the time the sound waves reach both ears, so the same result as in Fig. 23 is obtained.

6.2. Interaural level difference (ILD)

ILD is another important localization cue above 1.5 kHz. When a sound source deviates from the median plane, the sound pressure at the contralateral ear is attenuated, especially at high frequencies, due to the head shadow effect, while the sound pressure at the ipsilateral ear is amplified to some extent. In the far-field with distance r far larger than the head radius l , narrowband ILD is defined as follows:

$$ILD_{narr}(\theta, \phi, f) = 20 \log_{10} \left| \frac{H_R(\theta, \phi, f)}{H_L(\theta, \phi, f)} \right| \quad (24)$$

with $r \gg l$.

Here, each HRIR of 512 samples is zero-padded to 4,800 samples, and the frequency resolution is thus 10 Hz. ILD is a multivariate function of the frequency as well as the distance and direction of a sound source, but far-field ILD is almost independent of the distance of a sound source. Fig. 24(a) and (b) show the narrowband ILD contour map and its cutting plots with horizontal azimuths from -180° to $+180^\circ$ at several different frequencies. Comparing Fig. 23 and 24, unlike ITD, narrowband ILD may be an ambiguous localization cue because the ILD does not change monotonically with respect to azimuth.

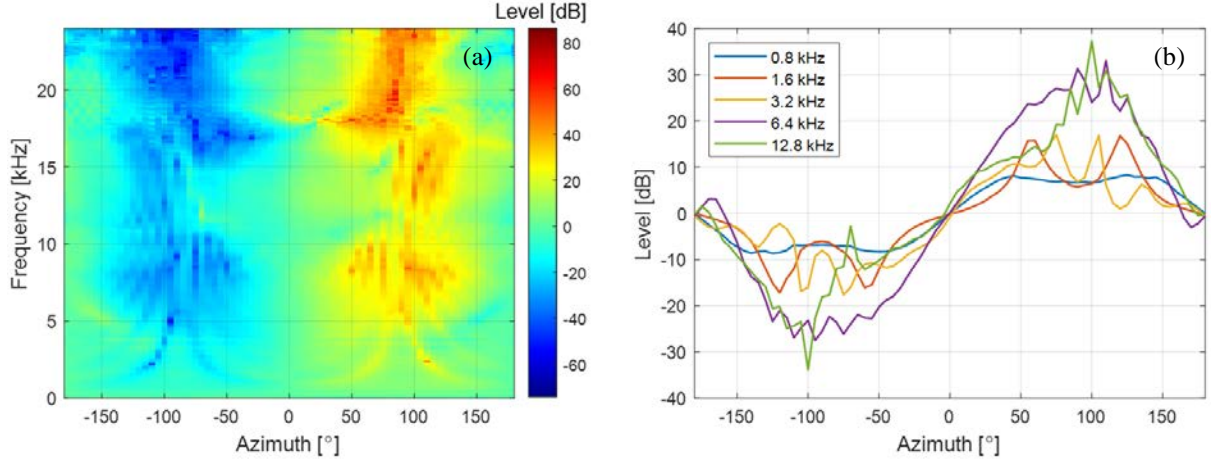


Fig. 24. Narrowband ILDs in the horizontal plane: (a) ILD contour map for all frequencies; (b) ILD plots for five frequencies.

The absolute value of ILD is nearly zero at the front and rear directions, and reaches the maximum around the lateral 90° directions. Fig. 24(b) illustrates that the ILD at 0.8 kHz has small level and changes smoothly with respect to azimuth, which indicates that the head shadow effect is negligible at low frequencies in the far-field. On the other hand, at high frequencies, the absolute value of ILD tends to increase and varies in a complex manner with respect to azimuth. At frequencies 1.6 kHz and 3.2 kHz, the maximum ILD does not appear at the azimuth of 90° where the sound source locates exactly opposite to the contralateral ear. This is because the sound pressure at the contralateral ear is enhanced by the in-phase interference of multi-path diffracted sound waves around the head. The sound pressure enhancement at the contralateral ear reduces the difference in sound pressure level with the ipsilateral ear, causing ILD notches at -90° and $+90^\circ$ in azimuth. As frequency increases, the wavelength of sound waves is shortened, so the bandwidth of the ILD notch becomes narrower. Therefore, above 5.0 kHz, the ILD notch becomes gradually insignificant, as shown in Fig. 24(a) and (b). The ILD curves are asymmetric with respect to $\pm 90^\circ$ above 3.2 kHz. This is caused by the front-back asymmetry of the head shape and ear position and the diffraction effect of the pinna. The front-back difference in the ILD curves is regarded as a localization clue to solve the front-back confusion in BSSL.

Although wideband ILD is not directly used as a binaural sound localization cue, it helps characterize the features of HRTF database. Wideband ILD can be obtained by implementing integration over the entire audio frequency range as [47]

$$ILD_{wide}(\theta, \phi) = 10 \log_{10} \left[\frac{\int_{f_L}^{f_H} |H_R(\theta, \phi, f)|^2 df}{\int_{f_L}^{f_H} |H_L(\theta, \phi, f)|^2 df} \right] \quad (25)$$

with $f_L = 20$ Hz; $f_H = 20$ kHz.

Fig. 25(a) and (b) plot the wideband ILD curves and contour map with azimuths from -180° to $+180^\circ$ and elevations from -40° to $+90^\circ$. Compared with Fig. 24, the variation in the wideband ILD according to azimuth is smaller than that in the high frequency narrowband ILD. The variation range of wideband ILD is maximum in the horizontal plane ($\phi = 0^\circ$) and decreases as the elevation angle of a sound source increases. At azimuths of -90° and $+90^\circ$, the ILD notch appears from -40° to $+30^\circ$ in elevation. At elevations outside this range, the variations of wideband ILD with azimuth become smooth as shown in the ITD curves. In addition, at elevation angles below 45° , the broadband ILD curves exhibit front-back asymmetry, which can be used as a localization cue to solve the front-back confusion in BSSL.

Considering the OTF measurement method, since the left and right HRTFs are normalized to the same OTF, the level difference between the left and right HRTFs is the same regardless of the OTF measurement method. Thus, ILD is not affected by OTF measurement method. As for the non-causality compensation, the magnitude responses of HRTF are the same before and after non-causality compensation as shown in Fig. 16(b1) and (b2). Therefore, ILD shows the same result as Fig. 25 regardless of the causality of HRTF.

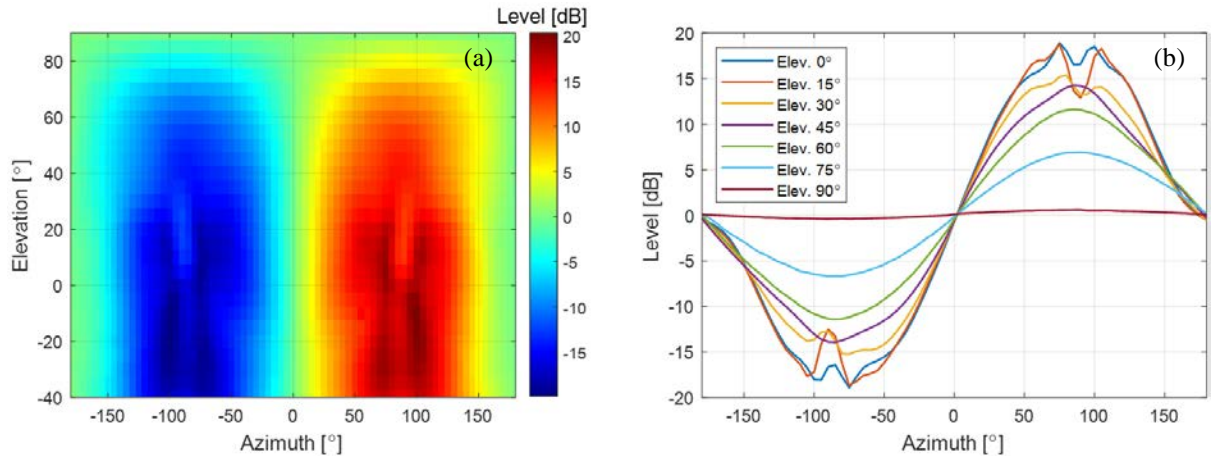


Fig. 25. Wideband ILDs that change with azimuth and elevation: (a) ILD contour map; (b) ILD plots for seven frequencies.

6.3. Spectral cue (SC)

The spectral features of sound pressure caused by reflection and diffraction of the pinna are important localization cues above 5 kHz [5]. The spectral features of the pinna can be analyzed via measured HRTFs. The high-frequency peaks and notches of HRTFs are reported to be generated in the pinna [6]. Specifically, it is considered that notches are generated in the cavity of concha [48], whereas peaks are generated by the resonance of the pinna [49]. Since first reported in Ref. [48], the elevation dependence of the pinna notch frequency has been considered an important vertical localization cue. To analyze the

vertical localization cue from the measured HRTF database, the patterns of peaks and notches according to elevation angles in the median plane were examined in this paper. For this purpose, pinna-related transfer functions (PRTFs), i.e., acoustic transfer functions related only to the pinna, were extracted from the measured HRTFs. Since the pinna response reaches the entrance of the ear canal before the torso response, the pinna influence is considered to be involved in the early part of HRIR. Thus, it is assumed that the information on the spectral peaks and notches of the pinna is included in the early part of HRIR. Since the early 1ms of HRIR contains information about the spectral peaks and notches for the pinna [6], HRIRs in the median plane are clipped by a 2 ms long Hanning window centered on the maximum sample of each HRIR, leaving only the pinna effect. Then, the windowed HRIRs were Fourier transformed to obtain PRTFs. To analyze SCs, the local maxima and minima of PRTFs were searched to obtain the distribution of peaks and notches according to frequency and elevation angle.

Fig. 26(a) shows the SC distribution of right PRTFs in the median plane with elevations from -40° to 220° . The peak at about 4 kHz is almost constant and is thus almost independent of the elevation angle of a sound source. This peak is called the first peak, P1, and is resulted from the modal response of the ear canal in the direction of depth. The second peak, P2, is formed around 10 kHz, and there is no significant change with the elevation angle. Since the P1 and P2 frequencies are almost independent of the elevation angle, the vertical localization cue is not included in the P1 and P2. On the other hand, the first notch, N1, and the second notch, N2, are highly dependent on the elevation angle of a sound source. In addition, the notches are deep for a sound source close to the horizontal plane and shallow for a source far from the horizontal plane. This elevation angle dependency of the N1 and N2 frequencies is thought to contribute as one of the vital cues for vertical localization. The N1 frequency is observed at about 8 kHz and changes from 8 kHz to 10 kHz, when elevation varies from -40° to 40° . The N2 frequency varies in a large amount as a sound source moves from 0° to 90° in elevation. This phenomenon explains why two notches are required for vertical localization. If the N1 and N2 frequencies change monotonically with the elevation angle of a sound source, two notches are not needed to determine the elevation angle. However, since the relationship between the notch frequencies and the elevation angle is not simple, at least two notches are required to determine the elevation angle of a sound source. Notably, the front-back asymmetry in the PRTF pattern provides an important localization clue to solve the front-back confusion of BSSL.

Fig. 26(b) shows the SC distribution of right PRTFs in the median plane, which is based on OTF measured by 90° off-axis microphone. As shown in Fig. 12(c), when OTF is measured with 90° off-axis microphone, the high-frequency level decreases compared to when OTF is measured with 0° on-axis microphone. Hence, HRTF based on 90° off-axis OTF has a higher level in the high frequency region than HRTF based on 0° on-axis OTF.

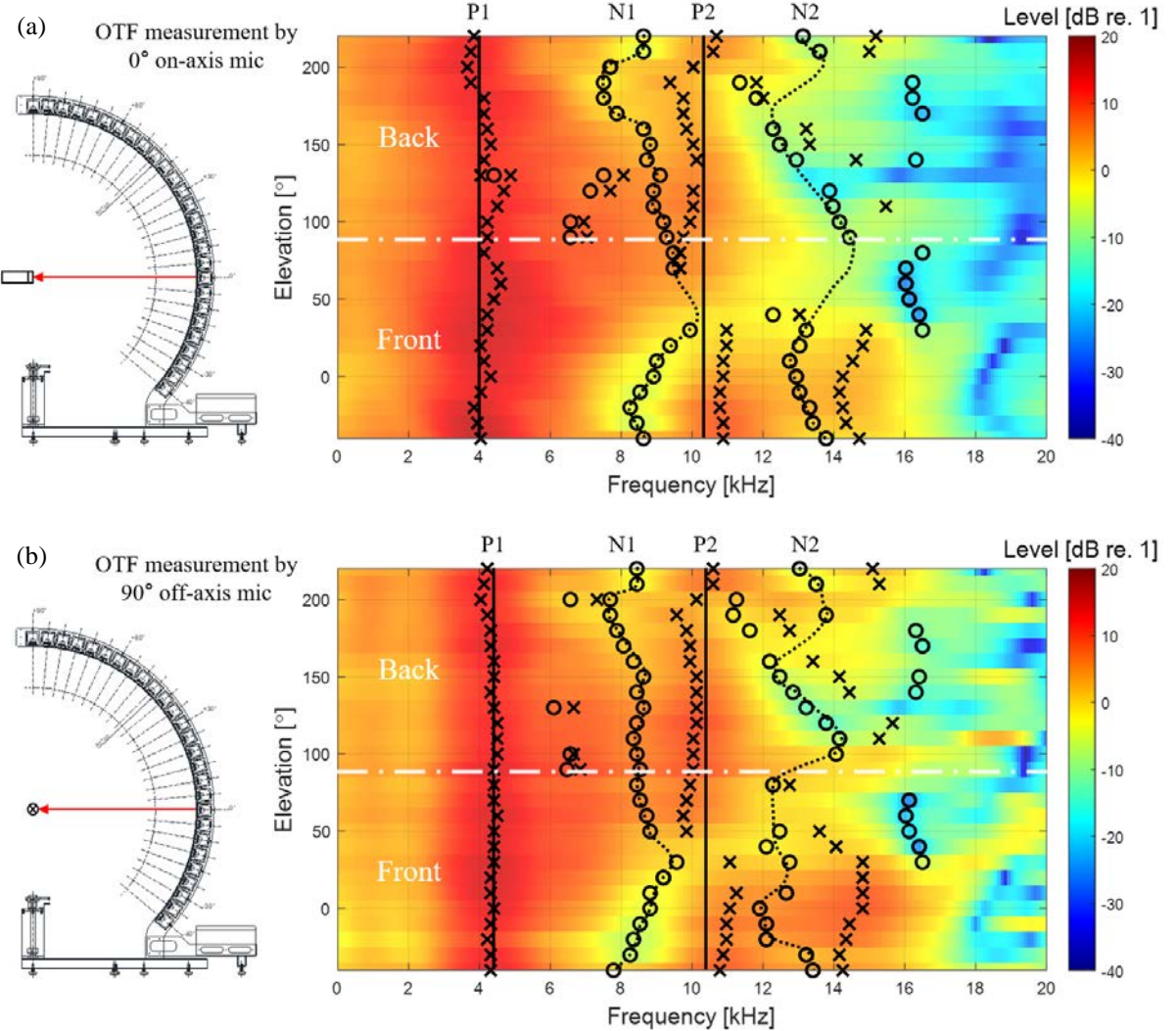


Fig. 26. SC distribution of right PRTFs in the median plane with elevations from -40° to 220° (X: peaks, O: notches): (a) SC distribution based on OTF measured by 0° on-axis mic; (b) SC distribution based on OTF measured by 90° off-axis mic.

This increase in the high-frequency level is also confirmed in the PRTF of Fig. 26. Moreover, as shown in Fig. 12(d), various peaks and notches exist in the level difference between 90° off-axis and 0° on-axis OTFs. These relative peaks and notches mean that the 90° off-axis OTF may affect the positions of the HRTF peaks and notches. In particular, the dominant peaks of 8 kHz and 12 kHz in the level difference affect the notch positions of HRTF. Comparing with N1 and N2 of Fig. 26(a), it can be seen that N1 and N2 of Fig. 26(b) are concentrated around 8 kHz and 12 kHz, respectively. As mentioned above, since the elevation dependency of the notch frequency is regarded as an important vertical localization cue, a change in notch frequencies of HRTF may confuse the elevation estimation. Considering the non-causality compensation, since the magnitude response of HRTF is the same

regardless of compensation, the peak and notch frequencies show the same pattern as in Fig. 26(a).

6.4. Horizontal plane directivity (HPD)

As mentioned above, the variations for ITD and ILD are maximized in the horizontal plane compared to other elevations, and spectral notches appear more pronounced for a sound source close to the horizontal plane. In general, it is known that human ability of localization is maximized in front of the horizontal plane [5]. Therefore, in the horizontal plane, the sensitivity patterns of the subject's left and right ears according to azimuth were obtained from the measured HRTFs and then investigated for each frequency. The beam pattern of HPD is defined by normalizing a HRTF in the horizontal plane by the HRTF in front of the horizontal plane as follows:

$$HPD_{L,R}(\theta, f) = 20 \log_{10} \left| \frac{H_{L,R}(\theta, 0, f)}{H_{L,R}(0, 0, f)} \right|. \quad (26)$$

Fig. 27 shows the left and right HPD beam patterns as a function of the azimuth of a sound source at different frequencies ($f = 0.75, 1.5, 3.0, 6.0$, and 12.0 kHz). Due to the front HRTF normalization, the HPD beam pattern at 0° is always 0 dB over the entire frequency range. Since the shape of the head is close to left-right symmetry, it is also observed in the HPD beam patterns. As in the narrowband ILD curves, it can be seen that the level difference between the left and right becomes larger as frequency increases for a sound source located on the side. The beam pattern at 0.75 kHz shows a smooth change between -5 dB and $+5$ dB. At 1.5 kHz and 3 kHz, directivity is formed as the main lobe gradually narrows in the ipsilateral direction, while it drops to -15 dB due to the head shadow effect in the contralateral direction.

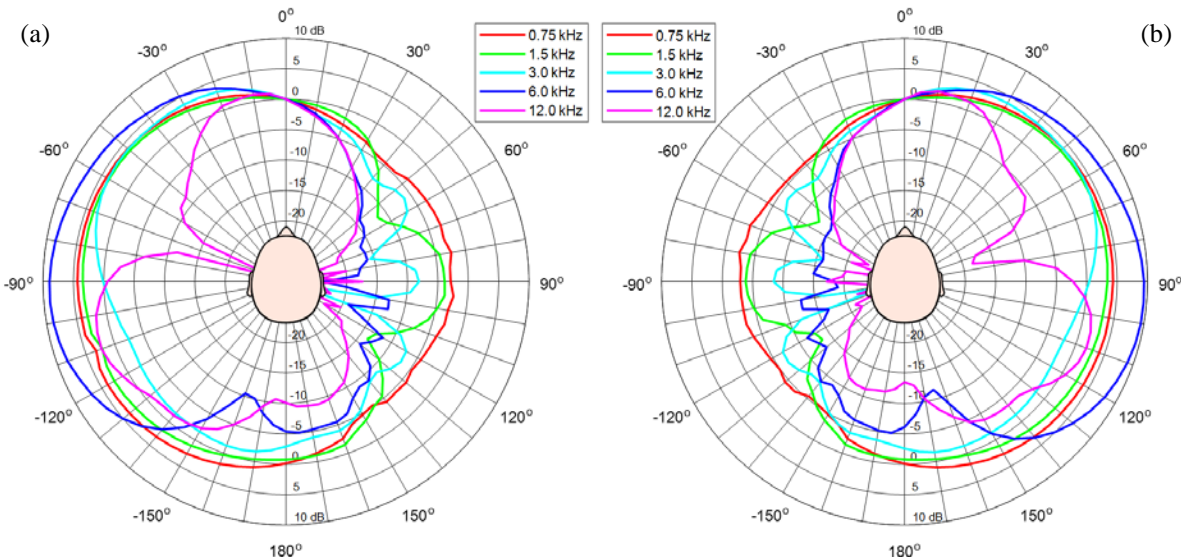


Fig. 27. Beam patterns of HPD: (a) left ear HPD beam pattern; (b) right ear HPD beam pattern.

The beam pattern at 6 kHz increases by about 10 dB in the ipsilateral direction while dropping by about –20 dB in the contralateral direction. At 12 kHz, a large dip appears at 70° in the ipsilateral direction, while it drops below –20 dB in the contralateral direction.

With regards to the OTF measurement method, since the HPD beam pattern is obtained by normalizing the horizontal HRTF to the front HRTF, the same result as in Fig. 27 appears no matter which OTF is used. In addition, since the magnitude response of HRTF is the same before and after the non-causality compensation, the HPD beam pattern is the same as in Fig. 27 regardless of whether the non-causality of HRTF is compensated.

7. Conclusions

Accurate and practical methods for the major issues of HRTF measurement was presented, especially on wideband speaker module design, measurement of the OTF at the head center, selection of time window interval, and compensation for non-causality of ipsilateral HRTF. Then, we investigated how these methods affected the binaural sound localization cues of HRTF.

In previous HRTF measurements, a speaker module was made without considering the band of interest, or a commercial speaker (not a single source) was used. Thus, it was hard to obtain accurate wideband HRTFs. However, the design of the speaker module for HRTF measurement is not difficult because it should be a 1-way sealed type which is the simplest of all loudspeaker types. By simulating its frequency response using the presented equivalent acoustic circuit, it is possible to design the speaker module quickly and accurately using only the TSPs of its speaker driver and the internal air volume of its speaker enclosure. Although the TSPs can be measured, approximate values can be obtained using the nominal TSPs presented in the specifications. Therefore, after obtaining the internal volume capable of reproducing the frequency band of interest through simulation, the speaker module can be simply designed based on it. Wideband sound localization cues can be obtained by measuring HRTF with the 1-way sealed speaker module that maximizes its frequency band in a limited space.

Since OTF is non-directional, it should be measured by pointing a microphone toward the acoustic on-axis of each speaker module. Conventional OTF measurement was conducted by a 0° on-axis or 90° off-axis microphone. When the microphone is tilted 90°, directivity appears in the radial direction of the microphone diaphragm, so the high frequency level is reduced by about 11 dB up to 20 kHz. In addition, since the magnitude response of the 90° off-axis OTF fluctuates compared to that of the 0° on-axis OTF, HRTFs derived by the 90° off-axis OTF may give erroneous spectral cues. Therefore, OTF should be measured by 0° on-axis microphone. However, it is cumbersome to redirect the microphone toward each speaker module every time to obtain the non-directional OTF. For this reason, the entire measurement section of the speaker array was divided into five sections considering the microphone's

omnidirectional range of about 30° . Then, the microphone was directed to the center of each section, and the OTF for each speaker module in the corresponding section was measured. The divided OTF measurement considering the on-axis microphone's omnidirectional range makes it possible to obtain the non-directional OTF while minimizing the number of microphone setups.

To extract only the essential information of a few milliseconds, the start and end points of the time window were set considering the propagation delay in the early part of each impulse response and the reflection in the later part of each impulse response, and then applied to each BIR and OIR. The start point was set as 1 ms before the maximum peak of the ipsilateral impulse responses, which is the most preceding impulse responses, to preserve the key information of BIR and OIR. To prevent comb filtering effects due to reflection, the end point was set as the first zero crossing point after 2.5 ms based on the maximum peak of each impulse response considering the shortest path of sound waves reflected from the measurement system. If the reflection is severe, it may affect SCs because periodic notches appear in the magnitude response of HRTF due to the comb filtering effect. By setting the end point based on the shortest reflection, it is possible to measure HRTF without the effect of reflection.

Since the ipsilateral HRIR is non-causal, its maximum sample appears later in the impulse response sequence due to the periodicity of the Fourier transform. Thus, ipsilateral HRIRs become discontinuous and cause excessive ITD changes. Thus, all HRIRs should be delayed to compensate for the discontinuity and to preserve the ITD information. When the azimuth is -90° or $+90^\circ$ in the horizontal plane, the arrival time difference of the sound waves between the head center and one of the ears becomes the maximum, and the maximum time difference is obtained by dividing the head radius by the speed of sound. Therefore, to compensate for the non-causality of ipsilateral HRIRs, all HRIRs were circular shifted by at least the maximum time difference.

As a result of analyzing the binaural sound localization cues such as ITD, ILD, SCs, and HPD encoded in HRTFs, we confirmed that presented methods have significant contributions for accurate identification of binaural sound localization cues. It is expected that the measured HRTF database will be used to create virtual acoustic scenes in VR and AR, and also be used for BSSL of humanoid robots with two ears. The MATLAB codes and technical documentation for building the HRTF database are available on GitHub (<https://github.com/hansaram80/HRTF-construction>) along with the database files such as ITD, ILD, SC data as well as the HRIR library.

Acknowledgements

This work was supported by “Human Resources Program in Energy Technology” of the Korea Institute of Energy Technology Evaluation and Planning (KETEP), granted financial resource from the Ministry of Trade, Industry & Energy, Republic of Korea. (No. 20204030200050), and also supported

by Korea Institute of Marine Science and Technology Promotion (KIMST) grant funded by the year 2022 Finances of Korea Ministry of Oceans and Fisheries (MOF) (Development of Technology for Localization of Core Equipment in the Marine Fisheries Industry, 20210623).

References

- [1] L. Rayleigh, XII. On our perception of sound direction, *Philosoph. Mag. Ser. 6* 13 (74) (1907) 214–232.
- [2] F.L. Wightman, D.J. Kistler, Headphone simulation of free-field listening. I: stimulus synthesis, *J. Acoust. Soc. Am.* 85 (2) (1989) 858–867.
- [3] H. Møller, Fundamentals of binaural technology, *Appl. Acoust.* 36 (1992) 171–218.
- [4] M. Kleiner, B.I. Dalenbäck, P. Svensson, Auralization—an overview, *J. Audio Eng. Soc.* 41 (11) (1993) 861–875.
- [5] B. Xie, Head-Related Transfer Function and Virtual Auditory Display, second ed., J. Ross Publishing, Plantation, 2013.
- [6] K. Iida, Head-Related Transfer Function and Acoustic Virtual Reality, Springer, Singapore, 2019.
- [7] M.R. Bai, K.Y. Ou, Head-related transfer function (HRTF) synthesis based on a three-dimensional array model and singular value decomposition, *J. Sound Vibr.* 281 (2005) 1093–1115.
- [8] D.R. Begault, 3-D Sound for Virtual Reality and Multimedia, Academic Press, Cambridge, MA, 1994.
- [9] R. Ranjan, W.S. Gan, Natural listening over headphones in augmented reality using adaptive filtering techniques, *IEEE/ACM Trans. Audio, Speech, Lang. Process.* 23 (11) (2015) 1988–2002.
- [10] C. Pang, H. Liu, X. Li, Multitask learning of time-frequency CNN for sound source localization, *IEEE Access* 7 (2019) 40725–40737.
- [11] Y. Yang, J. Xi, W. Zhang, L. Zhang, Full-sphere binaural sound source localization using multi-task neural network, in: 2020 Asia-Pacific Signal and Information Processing Association Annual Summit and Conference (APSIPA ASC), Auckland, New Zealand, December 7–10, 2020, pp. 432–436.
- [12] W.G. Gardner, K.D. Martin, HRTF measurements of a KEMAR, *J. Acoust. Soc. Am.* 97 (6) (1995) 3907–3908.
- [13] J. Blauert, M. Brüggen, K. Hartung, A.W. Bronkhorst, R. Drullmann, G. Reynaud, L. Pellieux, W. Krebber, R. Sottek, The AUDIS catalog of human HRTFs, *J. Acoust. Soc. Am.* 103 (5) (1998) 2901–2902.
- [14] V.R. Algazi, R.O. Duda, D.M. Thompson, C. Avendano, The CIPIC HRTF database, in: Proceedings of the 2001 IEEE Workshop on the Applications of Signal Processing to Audio and Acoustics (Cat. No.01TH8575), New York, NY, USA, October 21–24, 2001, pp. 99–102.

[15] Listen HRTF database. <http://recherche.ircam.fr/equipes/salles/listen/>, 2003 (accessed 08 October 2021).

[16] B. Xie, X. Zhong, D. Rao, Z. Liang, Head-related transfer function database and its analyses, *Sci. China Ser. G-Phys. Mech. Astron.* 50 (3) (2007) 267–280.

[17] P. Majdak, P. Balazs, B. Laback, Multiple exponential sweep method for fast measurement of head-related transfer functions, *J. Audio Eng. Soc.* 55 (7/8) (2007) 623–637.

[18] K. Watanabe, Y. Iwaya, Y. Suzuki, S. Takane, S. Sato, Dataset of head-related transfer functions measured with a circular loudspeaker array, *Acoust. Sci. & Tech.* 35 (3) (2014) 159–165.

[19] R. Bomhardt, M. de la Fuente Klein, J. Fels, A high-resolution head-related transfer function and three-dimensional ear model database, in: 172nd Meeting of the Acoustical Society of America, Honolulu, Hawaii, USA, November 28–December 02, 2016, pp. 1–11.

[20] T. Nishino, N. Inoue, K. Takeda, F. Itakura, Estimation of HRTFs on the horizontal plane using physical features, *Appl. Acoust.* 68 (8) (2007) 897–908.

[21] M. Zhang, W. Zhang, R.A. Kennedy, T.D. Abhayapala, HRTF measurement on KEMAR manikin, in: Proceedings of ACOUSTICS 2009, Adelaide, Australia, November 23–25, 2009, pp. 1–8.

[22] N. Gupta, A. Barreto, M. Joshi, J.C. Agudelo, HRTF database at FIU DSP Lab, in: 2010 IEEE International Conference on Acoustics, Speech and Signal Processing (ICASSP), Dallas, TX, USA, March 14–19, 2010, pp. 169–172.

[23] T. Carpentier, H. Bahu, M. Noisternig, O. Warusfel, Measurement of a head-related transfer function database with high spatial resolution, in: Forum Acusticum 2014, Krakow, Poland, September 7–12, 2014.

[24] N.D. Hai, N.K. Chaudhary, S. Peksi, R. Ranjan, J. He, W.S. Gan, Fast HRTF measurement system with unconstrained head movements for 3D audio in virtual and augmented reality applications, in: 2017 IEEE International Conference on Acoustics, Speech and Signal Processing (ICASSP), New Orleans, LA, USA, March 5–9, 2017, pp. 6576–6577.

[25] F. Denk, S.M.A. Ernst, J. Heeren, S.D. Ewert, B. Kollmeier, The Oldenburg Hearing Device (OlHeaD) HRTF Database, Technical Report Version 1.0.3, Department of Medical Physics and Acoustics, University of Oldenburg, Oldenburg, Germany, October 29, 2018, pp. 1–6.

[26] C. Armstrong, L. Thresh, D. Murphy, G. Kearney, A perceptual evaluation of individual and non-individual HRTFs: A case study of the SADIE II database, *Appl. Sci.-Basel* 8 (11) (2018) 1–21.

[27] J. He, R. Gupta, R. Ranjan, W.S. Gan, Non-invasive parametric HRTF measurement for human subjects using binaural and ambisonic recording of existing sound field, in: 2019 AES international conference on headphone technology, San Francisco, CA, USA, August 27–29, 2019, pp. 1–10.

[28] J. Reijniers, B. Partoens, J. Steckel, H. Peremans, HRTF measurement by means of unsupervised

head movements with respect to a single fixed speaker, *IEEE Access* 8 (2020) 92287–92300.

[29] H. Møller, M.F. Sørensen, D. Hammershøi, C.B. Jensen, Head-related transfer functions of human subjects, *J. Audio Eng. Soc.* 43 (5) (1995) 300–321.

[30] B. Masiero, M. Pollow, J. Fels, Design of a fast broadband individual head-related transfer function measurement system, in: *Forum Acusticum 2011*, Aalborg, Denmark, June 27–July 1, 2011.

[31] G. Yu, R. Wu, Y. Liu, B. Xie, Near-field head-related transfer-function measurement and database of human subjects, *J. Acoust. Soc. Am.* 143 (3) (2018) EL194–EL198.

[32] J.G. Richter, J. Fels, On the influence of continuous subject rotation during high-resolution head-related transfer function measurements, *IEEE-ACM Trans. Audio Speech Lang.* 27 (4) (2019) 730–741.

[33] M. Pec, M. Bujacz, P. Strumiłło, A. Materka, Individual HRTF measurements for accurate obstacle sonification in an electronic travel aid for the blind, in: *2008 International Conference on Signals and Electronic Systems*, Krakow, Poland, September 14–17, 2008, pp. 235–238.

[34] H.F. Olson, Direct radiator loudspeaker enclosures, *J. Audio Eng. Soc.* 0 (1) (1951) 34, 36, 38, 59–64.

[35] D. Son, Y. Park, Y. Park, S. Jang, Building Korean head-related transfer function database, *Trans. Korean Soc. Noise Vib. Eng.* 24 (4) (2014) 282–288.

[36] J. Blauert, *Spatial Hearing: The Psychophysics of Human Sound Localization*, second ed., MIT Press, Cambridge, 1997.

[37] K. Riederer, M. Karjalainen, DSP aspects of HRTF measurements, in: *1998 IEEE Nordic Signal Processing Symposium*, Vigsø, Denmark, June 8–11, 1998, pp. 185–188.

[38] S. Takane, D. Arai, T. Miyajima, K. Watanabe, Y. Suzuki, T. Sone, A database of head-related transfer functions in whole directions on upper hemisphere, *Acoust. Sci. & Tech.* 23 (3) (2002) 160–162.

[39] B.P. Bovbjerg, F. Christensen, P. Minnaar, X. Chen, Measuring the head-related transfer functions of an artificial head with a high directional resolution, in: *109th Audio Engineering Society Convention*, Los Angeles, CA, USA, September 22–25, 2000.

[40] T. Snaidero, F. Jacobsen, J. Buchholz, Measuring HRTFs of Brüel & Kjær Type 4128-C, G.R.A.S. KEMAR Type 45BM, and Head Acoustics HMS II.3 Head and Torso Simulators, Technical Report, Department of Electrical Engineering, Technical University of Denmark, Lyngby, Denmark, March 29, 2011, pp. 1–45.

[41] D. Nikolic, S.Y. Kim, R. Allen, Identification of sound-localization cues in the HRTF of the bat-head model, *Biomed. Signal Process. Control* 7 (3) (2012) 270–277.

[42] L.E. Kinsler, A.R. Frey, A.B. Coppens, J.V. Sanders, *Fundamentals of Acoustics*, fourth ed., John Wiley & Sons, Inc., New York, Chichester, Weinheim, Brisbane, Singapore, Toronto, 2000.

[43] E. Grassi, J. Tulsi, S. Shamma, Measurement of head-related transfer functions based on the empirical transfer function estimate, in: Proceedings of the 2003 International Conference on Auditory Display, Boston, MA, USA, July 6–9, 2003, pp. 119–122.

[44] M. Morimoto, H. Aokata, Localization cues of sound sources in the upper hemisphere, *J. Acoust. Soc. Jpn. (E)* 5 (3) (1984) 165–173.

[45] J.C. Makous, J.C. Middlebrooks, Two-dimensional sound localization by human listeners, *J. Acoust. Soc. Am.* 87 (5) (1990) 2188–2200.

[46] L.L. Beranek, T.J. Mellow, *Acoustics: Sound Fields and Transducers*, first ed., Academic Press, Amsterdam, Boston, Heidelberg, London, New York, Oxford, Paris, San Diego, San Francisco, Singapore, Sydney, Tokyo, 2012.

[47] W.G. Gardner, *3-D Audio Using Loudspeakers* (Ph.D. Thesis), Massachusetts Institute of Technology, USA, 1997.

[48] E.A.G. Shaw, R. Teranishi, Sound pressure generated in an external-ear replica and real human ears by a nearby point source, *J. Acoust. Soc. Am.* 44 (1) (1968) 240–249.

[49] H. Takemoto, P. Mokhtari, H. Kato, R. Nishimura, K. Iida, Mechanism for generating peaks and notches of head-related transfer functions in the median plane, *J. Acoust. Soc. Am.* 132 (6) (2012) 3832–3841.